Journal of Materials Chemistry B

ROYAL SOCIETY OF CHEMISTRY

PAPER

View Article Online
View Journal | View Issue



Cite this: J. Mater. Chem. B, 2024, 12, 9622

# Liquid–liquid phase transition as a basis for novel materials for skin repair and regeneration

Shunfeng Wang, †[a] Meik Neufurth, †[a] Hadrian Schepler,[b] Rafael Muñoz-Espí,[c] Hiroshi Ushijima,[d] Heinz C. Schröder,[a] Xiaohong Wang *[a] and Werner E. G. Müller *[a]

Inorganic materials are of increasing interest not only for bone repair but also for other applications in regenerative medicine. In this study, the combined effects of energy-providing, regeneratively active inorganic polyphosphate (polyP) and also morphogenetically active pearl powder on wound healing were investigated. Aragonite, the mineralic constituent of pearl nacre and thermodynamically unstable form of crystalline calcium carbonate, was found to be converted into a soluble state in the presence of a $Ca^{2+}$-containing wound exudate, particularly upon addition of sodium polyP (Na-polyP), driven by the transfer of $Ca^{2+}$ ions from aragonite to polyP, leading to liquid–liquid phase separation to form an aqueous Ca-polyP coacervate. This process is further enhanced in the presence of Ca-polyP nanoparticles (Ca-polyP-NP). Kinetic studies revealed that the coacervation of polyP and nacre aragonite in wound exudate is a very rapid process that results in the formation of a stronger gel with a porous structure compared to polyP alone. Coacervate formation, enabled by phase transition of crystalline aragonite in the presence of Na-polyP/Ca-polyP-NP and wound exudate, could also be demonstrated in a hydroxyethyl cellulose-based hydrogel used for wound treatment. Furthermore, it is shown that Na-polyP/Ca-polyP-NP together with nacre aragonite strongly enhances the proliferation of mesenchymal stem cells and promotes microtube formation in the *in vitro* angiogenesis assay with HUVEC endothelial cells. The latter effect was confirmed by gene expression studies, applying real-time polymerase chain reaction, using the biomarker genes VEGF (vascular endothelial growth factor) and hypoxia-inducible factor-1 α (HIF-1α). Division of Escherichia coli is suppressed when suspended in a matrix containing Na-polyP/Ca-polyP-NP and aragonite. The potential medical relevance of these findings is supported by an animal study on genetically engineered diabetic mice (db/db), which demonstrated a marked increase in granulation tissue and microvessel formation in regenerating experimental wounds treated with Ca-polyP-NP compared to controls. Co-administration of aragonite significantly accelerated the wound healing-promoting effect of polyP in db/db mice. Based on these results, we propose that the ability of polyP to form a mixed coacervate with aragonite, in addition to its energy (ATP)-generating function, can decisively contribute to the regenerative activity of this polymer in wound repair.



Received 18th May 2024,
Accepted 3rd August 2024

DOI: 10.1039/d4tb01080a

rsc.li/materials-b

## 1. Introduction

Advanced products for skin repair and regeneration make use of the whole range of skin protective materials available for the treatment of acute, critical and chronic wounds, from materials used for treatment of venous leg ulcers, diabetic foot ulcers, pressure ulcers, burns and post-operative wounds.[1] They also include regeneratively active skin creams that reinforce the protective potency of the skin, the largest organ of the body, against external influences, microorganisms, fungi and viruses. Their aim is in particular to prevent and act as a protective barrier against external pathogens from entering the body *via* the bloodstream. The physiological, innate immune system

[a] *ERC Advanced Investigator Grant Research Group at the Institute for Physiological Chemistry, University Medical Center of the Johannes Gutenberg University, Duesbergweg 6, 55128 Mainz, Germany. E-mail: wang013@uni-mainz.de, wmueller@uni-mainz.de*
[b] *Department of Dermatology, University Medical Center of the Johannes Gutenberg University, Langenbeckstraße 1, 55131 Mainz, Germany*
[c] *Institute of Materials Science (ICMUV), Universitat de València, C/Catedràtic José Beltrán 2, 46980 Paterna-València, Spain*
[d] *Nihon University, Division of Microbiology, Department of Pathology and Microbiology, Nihon University-School of Medicine, Tokyo, Japan*
† These authors contributed equally to this paper.

of the skin eliminates most of these pathogens and prevents the human body from cutaneous and systemic infections.[2] The regenerative potential of advanced skin repair products prevents superficial wounds from developing into chronic wounds or even chronic skin ulcers. The healing process in these progressed clinical pictures is disrupted in patients suffering from venous stasis, diabetes mellitus or other chronic insufficiencies.

Advanced products for skin repair meet these requirements at least partially due to their active constituents, such as anti-inflammatory, moisturizing and cleansing ingredients. However, the formulations applied usually lack compounds that provide the cells with a metabolic fuel that can substitute the deficiency of energy in the extracellular space and body fluids. Certainly, the energy status of the skin is a prominent factor in skin defense,[3] and more specifically, it is the mitochondria in particular that play an essential role in regulating the ATP homeostasis in skin physiology.[4] This nucleotide is considered the most important intracellular energy-providing metabolite due to its two high-energy anhydride bonds and is the driving force for exergonic reactions. After enzymatic cleavage, 30.5 kJ $mol^{-1}$ of energy is released per energy-rich bond in the ATP molecule.[5] It is important to stress that the intracellular ATP pool is high at 3–10 mM, while the extracellular ATP levels are only ≈10 nM.[6,7] However, in every living organism and certainly also in humans,[8] there is another high-energy molecule in addition to ATP, namely inorganic polyphosphate (polyP).[9,10] Importantly, while ATP only has two high-energy bonds, polyP with a physiological chain length of ≈100 $P_i$ (phosphate) units[11] contains a much larger number of energy-rich phosphoanhydride linkages. On a molar base, the energy density in this polymer is 50 times higher than that in ATP.[12] The highest concentration of polyP in humans and other mammalian organisms is found in the blood platelets, encapsulated in the dense granules of these cell fragments in addition to large amounts of ADP and ATP as well as pyrophosphate.[13,14]

The polyP in platelets serves as ATP generator. The free energy stepwise released during the successive enzymatic degradation of the polymer with alkaline phosphatase (ALP) is first stored in ADP, followed by the up-phosphorylation of ADP to ATP by adenylate kinase (ADK).[12] These two enzymes are exposed on the outer cell surface.[15] It is also noteworthy that polyP not only functions as an ATP generator extracellularly, but also positively affects intracellular ATP generation. After entry into the cells, probably coupled to ion transport,[16] polyP causes a significant accumulation of mitochondria,[15] resulting in an increased ATP formation through the mitochondrial $F_oF_1$-ATP synthase system.[17]

The property of polyP to act as a generator for the metabolic fuel ATP is enhanced by its property to transform into a coacervate phase (Fig. 1) in the presence of divalent cations such as $Ca^{2+}$ or $Mg^{2+}$, whereby polyP and the cations undergo a liquid–liquid phase separation with a denser polyP-rich phase and a phase rich in $Ca^{2+}$ or $Mg^{2+}$.[18,19] Liquid–liquid phase separation in a polymer-rich and polymer-poor phase has been considered as the second step during complex coacervation.[20,21] In the coacervate stage, the polymers can be exploited for their

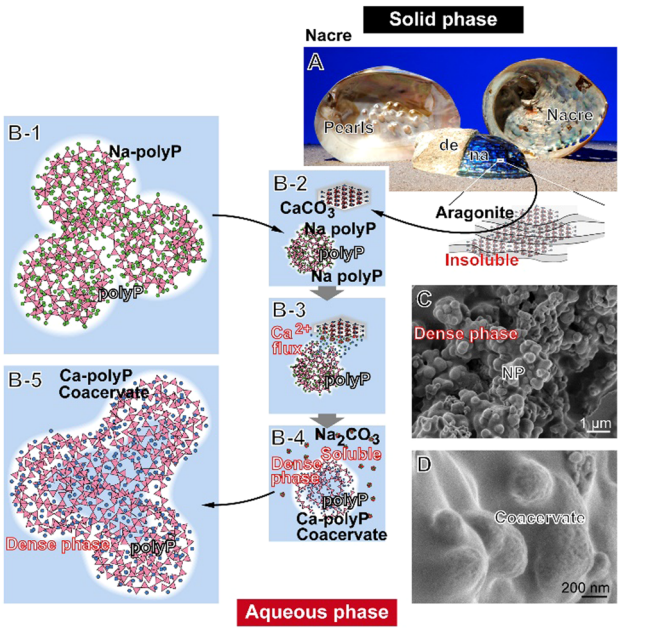


Fig. 1 Conversion of solid aragonite into an aqueous coacervate phase in the presence of Na-polyP. (A) Nacre (na) stretched inside of bivalve shells, produces pearls when injured. Also on the outer surface of the shells, Ca-carbonate deposits (de) are formed on the nacre platform. (B-1) After coming into contact with Na-polyP, (B-2) the aragonite material dissociates into $Ca^{2+}$ and $CO_3^{2-}$, (B-3) allowing a $Ca^{2+}$ flux, (B-4) followed by the formation of soluble Na-carbonate ($Na_2CO_3$) and denser Ca-polyP coacervate droplets, (B-5) ending up with a voluminous aqueous Ca-polyP coacervate. (C) Ca-polyP nanoparticles (Ca-polyP-NP); SEM. (D) Like aragonite, the Ca-polyP-NP, which form a nearly indissoluble dense phase, undergo coacervation when suspended in peptide-containing medium/serum; ESEM.

inherent biological potency.[22] Furthermore, during the process of coacervation, microbial cells can be enveloped and ultimately killed.[23] A final remarkable property of polyP is that the polymer can stabilize the amorphous phase of Ca-carbonate[24] and can thereby preserve the biological/osteogenic activity of Ca-carbonate even in its nanoparticulate form.[25]

The morphogenetic, regeneration-activating activity of polyP is well established[26–28] and has been proven in a proof-of-concept study even for human application.[23,29] For the Ca-polyP used, it is evident that the $Ca^{2+}$ ions are essential for regeneration.[30] As outlined above, the polyP backbone with its high-energy phosphoanhydride bonds provides the metabolic energy source for any cell-based regeneration process.[12]

In addition to its property to stabilize amorphous Ca-carbonate and decelerate the crystallization process from amorphous to crystalline Ca-carbonate, polyP also enhances the beneficial effect of calcium on wound healing.[31] In the amorphous state, the $Ca^{2+}$ ions promote the healing of skin wounds, especially chronic wounds, by activating the proliferation, differentiation and migration of keratinocytes as well as the proliferation and collagen deposition of fibroblasts.[32,33] Furthermore, preliminary data suggest that carbonate also promotes wound healing.[34] Carbonate can be released from the less stable form of crystalline Ca-carbonate, from aragonite,

which subsequently buffers the systems.[35] Previously, it was reported that soluble Na-carbonate is able to form spherical coacervate droplets with a size of ≈200 nm in the presence of $Ca^{2+}$.[36] In turn, we postulated that aragonite, as the thermodynamically unstable phase of crystalline Ca-carbonate, could also form coacervate deposits like Ca-polyP. A biomaterial that consists of >95% aragonite is nacre/pearls, which is formed by freshwater bivalve molluscs such as from the hybrid species (*Hyriopsis schlegeli*/*Hyriopsis cumingi*) as an inner shell layer.[37–39] For biomedical application, the formulation as pearl powder is frequently used.[40] It is interesting and suggestive that the nacre (Fig. 1(A)), the smooth outer shell surfaces, can serve as a platform for mineralization of nanoscale amorphous and crystalline Ca-carbonate mineral precursors.[41] Pearl medicine has a history of over 2000 years in both Europe and Asia, and pearls are used in Europe in therapy of skin sufferings, as mentioned by Vallés,[42] as medical cleansing agents [de compositione medimecatorum expurgantium] for treatment of skin diseases [podest nunc exmodo morbi]. An even wider application is reported from China, in which the powder is used, for example, to calm the mind, clear the eyes or detoxify organs.[43]

The aim of the present study was to combine the energy-generating and regeneratively active potential of polyP with the inherent morphogenetic activities of pearl powder.[44] This mineralic material, in the nanoparticle (NP) form, stimulates human mesenchymal stem cells (MSC), promotes osteogenic differentiation *in vitro* by inducing the ALP activity and causes an upregulation of genes. Moreover, pearl powder implanted into the dermis of rats causes an activation of skin fibroblasts, in parallel with an enhanced extracellular matrix synthesis and the organization of the filamentous structures and, associated with this, the formation a dense network rich in collagen I and collagen III.[25,45] Slices of pearl powder, seeded with MSC start to secrete ALP in an extent that exceeds the level induced by bone morphogenetic protein (BMP-2) treatment.[46]

Originally, it was reported that activated platelets release polyP with a chain length of 60–100 $P_i$ residues, which initiate the blood clotting contact pathway.[47] However, later it was argued to the contrary that this effect is not relevant.[48] The technical difficulty is that polyP in the circulating blood is enzymatically hydrolyzed by ALP, which shortens the chain lengths of the polymer.[49] It has been reported that very long polyP molecules (>500 $P_i$ units), such as those found in microorganisms, interfere with the blood clotting cascade, while shorter polymers do not exhibit this property.[50] It is most likely that polyP is released from the platelets either as Na-polyP or as Ca-polyP-NP[51] due to the high $Ca^{2+}$ level in the platelets.[52,53] The Ca-polyP-NP with the divalent metal ions remain on the surface of the platelets as insoluble spherical nanoparticles. For chemical synthesis of Ca-polyP, a sintering procedure is usually used, which usually ends up in the crystalline form of the material.[54] Likewise, the second component mixed with polyP, the nacreous aragonite, exists in the crystalline aragonite phase.[37]

However, in order to exploit the biomedical potential of the basically solid aragonite with its excellent strength and toughness for bio-medical skin repair, such as in acute and chronic wounds, the powder must be converted into a soluble phase. In this state, pearl powder exhibits distinct wound healing activity by promoting cell migration and inducing the expression of type III collagen.[55]

The concept, which has been experimentally proven, is outlined here and is achieved by immersing the crystalline aragonite in a nonbuffered Na-polyP solution as sketched (Fig. 1). Solid aragonite (Fig. 1(A)) is converted into the soluble form upon immersion together with Na-polyP (Fig. 1(B-1)), a soluble and weakly basic salt that dissociates into $Na^+$ cations and polyP anions.[56] In medium/serum, the $Ca^{2+}$ ions from aragonite (Ca-carbonate) are then chelated by Na-polyP, resulting in the conversion of the solid phase into an aqueous Ca-polyP coacervate (Fig. 1(B-2)–(B-5)). If the incubation system contains Ca-polyP-NP, which are characterized by a high zeta potential,[18] the coacervate formation is amplified due to the conversion of the fairly indissoluble NP into a soluble state. It can be assumed that such a process also occurs in the presence of body fluids such as sweat and wound secretions, which are rich in peptides/proteins and $Ca^{2+}$,[57] components that affect and lower the high zeta potential[18] of the indissoluble polyP particles [dense phase] (Fig. 1(C)) and transform them into the more fluid, aqueous coacervate (Fig. 1(D)).

In the present contribution, this concept of producing a co-coacervate from calcareous nacre of pearls and Na-polyP is experimentally supported and it is shown that the mixed coacervate phases (Ca-carbonate/Na-polyP) accelerate the proliferation of MSC and trigger the subsequent organization of these cells for microtube formation, the onset of blood vessel formation. These results are further supported by reverse transcription-quantitative real-time polymerase chain reaction (RT-qPCR) using the biomarker genes VEGF (vascular endothelial growth factor) and hypoxia-inducible factor-1α (HIF-1α). The VEGF is a pivotal proangiogenic regulator of angiogenesis,[58] while HIF-1α is the oxygen-regulated subunit that determines HIF-1 activity.[59] Both genes are strongly expressed during angiogenesis.[59]

## 2. Experimental section

### 2.1. Components

Crushed powdered pearls (aragonite) were purchased from Dura Green (Nanjing; China); the particles had a size from 3 to 10 μm. The freshwater mussel hybrid species (*Hyriopsis schlegeli*/*Hyriopsis cumingi*) has been used to obtain the pearls; they were cultured in the pearl farm in Zhuji (Zhejinag, China). There, a rectangular piece of mantle tissue was routinely prepared from the interior of their shells and reinserted into the mantle epithelium, where a pearl sac is formed and initiates the deposition of the aragonite structure of the shell.[60] The shape of the pearls is caused by the shape of the inserted implant.

Na-polyphosphate (Na-polyP) with an average chain length of 40 $P_i$ units was purchased from Chemische Fabrik Budenheim (Budenheim; Germany).

 

### 2.2. Preparation of Ca-polyP-NP

Amorphous Ca-polyP nanoparticles (Ca-polyP-NP) were prepared from Na-polyP and $CaCl_2$ (#A537.1; Roth, Karlsruhe; Germany) as described.[61] A 1 : 3 weight ratio of both components was used as start concentration.

### 2.3. Application forms

PolyP (either Na-polyP or Ca-polyP-NP) with or without pearl powder was applied to the system either directly or supplemented with a hydrogel or wound exudate removed from human chronic wounds.[29] The samples were collected in accordance with the rules of the declaration of Helsinki. In addition to these recommendations, the consent of the patients has been granted. The respective weight ratio is given with the corresponding experiments. If not mentioned otherwise, a 1 : 1 weight ratio between polyP and aragonite (pearl powder) was used.

### 2.4. Hydrogel-based gel formulation

The formulation of the polyP-containing hydrogel was prepared as outlined before.[23] The hydrogel consisted of a 2% (wt/wt) hydroxyethyl cellulose (Caelo, Hilden; Germany) solution prepared with 10% (wt/wt) 1,2-propandiol (#2554; Caelo). The system was buffered with phosphate buffer to pH 6.5. If indicated, a polyP suspension (200 mg of Na-polyP and 20 mg of Ca-polyP-NP per 10 mL) was prepared and added to the hydrogel. The final formulation contained 600 μg $mL^{-1}$ of Na-polyP and 60 μg $mL^{-1}$ of Ca-polyP-NP.

### 2.5. Analytical methods

**Fourier transformed infrared spectroscopy.** After drying, the sample material was ground to a composite powder and analyzed by FTIR (Fourier Transformed Infrared Spectroscopy). An attenuated total reflectance-FTIR spectroscope/Varian IR spectrometer (Agilent, Santa Clara; CA) hooked to a Golden Gate ATR unit (Specac, Orpington; UK) was used.

**X-ray diffraction analysis.** For XRD analyses, the dried powder samples were inspected with a D8 Advance A25 diffractometer (Bruker, Billerica; MA). The instrument was connected with a monochromatic Cu-$K_\alpha$ radiation system.

### 2.6. Cell biological studies

***In vitro* angiogenesis assay.** The studies were performed with human umbilical vein endothelial cells (HUVEC) purchased from Lonza (Basel; Switzerland). The cells were cultured in endothelial growth medium with 4% (v/v) fetal bovine serum (FBS; #F7942, Sigma) together with 0.4% bovine brain extract (BBE; #CC-4098, Lonza).[62] The *in vitro* tube formation assay (Cultrex *in vitro* Angiogenesis Assay Kit; Trevigen, Gaithersburg: MD) was used according to the instructions of the manufacturer and as described.[63] The $Ca^{2+}$ concentration in the system was 1.5 mM. The plates were coated with Reduced Growth Factor Basement Membrane Extract (Trevigen) and wound exudate enriched either with a polyP cocktail (final concentration in the assay, 100 μg $mL^{-1}$ of Na-polyP and 20 μg $mL^{-1}$ of Ca-polyP-NP) or a polyP plus aragonite (120 μg $mL^{-1}$) mixture, as indicated in the respective experiments. This arrangement was overlayed with HUVEC at a density of $5 \times 10^3$ cells per $cm^2$ in 24-well plates.

**Determination of cell proliferation.** The determination of the effect of polyP and aragonite (nacre) on cell proliferation was performed with human MSC (mesenchymal stem cells). The cells were cultivated as outlined[64] and obtained from healthy nondiabetic donors; they were obtained from Lonza Cologne (Cologne; Germany). The MSC were propagated in Dulbecco's Modified Eagle Medium (DMEM) medium, supplemented with 10% FCS (fetal calf serum) (Biochrom, Berlin; Germany). After passage to a density of $5 \times 10^3$ cells $cm^{-2}$ in 24-well tissue culture plates, the cells were incubated for a period of up to 8 d. During this period, the medium/serum was supplemented either with the polyP cocktail Na-polyP (100 μg $mL^{-1}$) together with Ca-polyP-NP (20 μg $mL^{-1}$) or a mixture of this polyP suspension with aragonite (120 μg $mL^{-1}$) in a ratio of 1 : 1 (wt/wt). After termination, the cell proliferation was assessed microscopically by staining with Calcein AM (#223506; Sigma) and visualized microscopically.[65]

A quantitative determination was achieved by staining with the cell viability reagent PrestoBlue (Life Technologies, Dreieich; Germany) at the end of the incubation; the relative fluorescence units (RFU) were determined at 570 nm and for reference at the wavelength of 595 nm.[66] Ten parallel experiments were performed; data are means ± SD ($P < 0.01$).

In another series of experiments to determine the effect of the hydrogel without or with supplements on cell morphology, 300 μL MSC cultures, in the middle of exponential growth phase ($150 \times 10^3$ cells $mL^{-1}$), were added to 100 μL of wound exudate and 100 μL of hydrogel either containing no polyP or aragonite or supplemented with the polyP suspension (final concentration in the assay 120 μg $mL^{-1}$ of Na-polyP) together with aragonite (final concentration: 120 μg $mL^{-1}$). The system was buffered with a phosphate buffer to pH 6.5. The cultures were incubated for 12 h; then the cells were freeze-died and inspected by SEM.

**Cultivation and exposure of bacteria.** *Escherichia coli* M15 strain cells were grown in LB medium (Qiagen, Hilden; Germany) as described.[67] After reaching the exponential growth phase, the bacterial cultures either remained free of further additions or were supplemented with 100 μl $mL^{-1}$ LB medium containing the polyP cocktail (100 μg $mL^{-1}$ of Na-polyP and 20 μg $mL^{-1}$ of Ca-polyP-NP) together with aragonite (120 μg $mL^{-1}$). If indicated, wound exudate was added. After incubation for overnight, 100 μL samples were taken, placed onto grids, and dried by critical point freezing.[68]

The bacterial suspensions were centrifuged at 1700 × *g* for 10 min (Centrifuge 5810R, Eppendorf, Germany) to separate bacterial pellets. After removing the supernatant, the pellets were rinsed in 3 mL of distilled water (Bio-Rad Laboratories, United States), followed by a second centrifugation under the same conditions. Five to 10 μL of condensed bacterial suspensions were collected.

The condensed bacterial suspension was applied to the surface of a 15 mm × 35 mm Silicon (Si) wafer (Siltronix, France) and

dried under a biosafety hood. Dried spots of bacterial deposits with a typical thickness of 5–15 μm were obtained depending on the bacterial concentration after rinsing.

Optical density ($OD_{600}$) measurements were performed to determine the effect of the polyP/aragonite coacervate on the growth of *E. coli*. Bactericidal kinetics were measured at an optical density (OD) of 600 nm. *E. coli* [$\sim 10^6$ cfu $mL^{-1}$] suspended in 5 mL bacterial culture were shaken overnight at 30 °C. Aliquots of 100 μL were removed at different time intervals and the respective densities were measured.[69]

**Reverse transcription-quantitative real-time PCR analyses.** The technique of RT-qPCR was applied to determine the gene expression levels of VEGF and HIF-1α in human HUVEC. Cells were incubated as described above. The RT-qPCR reaction and evaluation were performed as published earlier.[70,71] After collection of the cells, RNA was isolated and subjected to RT-qPCR to determine the expression levels of HIF-1α and VEGF. The following primer pairs were used to amplify HIF-1α; the forward primer TATGACCTGCTTGGTGCTGA and the reverse primer GGGAGAAAATCAAGTCGTGC at an annealing temperature of 60 °C. For amplification of the VEGF, the forward primer AACTTTCTGCTGTCTTGG and the reverse primer TTTGGTC TGCATTCACAT were used at an annealing temperature of 55 °C.[72]

For the amplification of the glyceraldehyde-3-phosphate dehydrogenase (GAPDH) housekeeping gene, the forward primer GTCTCCTCTGACTTCAACAGCG and the reverse primer ACCACCCTGTTGCTGTAGCCAA were selected.[73] The annealing temperature was 62 °C. The amplifications were performed in an iCycler (Bio-Rad, Hercules, CA, USA) with the respective iCycler software. Finally the $C_t$ values of the expressions of the respective transcripts were calculated.[74]

### 2.8. Animal experiments

**Ethics.** All animal-related research was conducted in accordance with 2010/63/EU and national legislation regulating the use of laboratory animals in scientific research and for other purposes (Official Gazette 55/13; Pursuant to Article 89 of the Constitution of the Republic of Croatia [Zagreb, 10 October 2017]). All experiments conducted in the study described herein were performed under the institutional ethics committee approval number CAREZG_13-06-14_49 EP/2016 (SP-167-15 and SP-167-16). The approval number from the Ministry of Agriculture, Republic of Croatia was KLASA: UP/I-322-01/15-01/108, URBROJ: 525-10/0255-16-8.

Details comprising the animal studies have been given earlier.[75]

**Experimental procedures for wound-healing studies.** The experimental studies summarized here were performed with male diabetic mice (mean blood glucose level: 527 ± 9 mg $dL^{-1}$) with the genetic background 000700 BKS.Cg-Dock7$^{m}$ Lepr$^{db}$/++/J, originating from a spontaneous mutation at the Lepr locus on a C57BLKS/J background. In comparison, common inbred strain of laboratory mouse, male C57BL/6, were included in the study. The animals had an age of 6 to 7 weeks and were purchased from Charles River (Calco, Italy). Per group, six to eight animals were included. After shaping the interscapular region and disinfection, single full-thickness excisional wounds, 8-mm in diameter, were punched. Postoperative pain control was applied through daily s.c. injections of 4 mg $kg^{-1}$ carprofen (5% Norocarp; Pfizer, USA) in sterile, deionised water. The animals were sacrificed after intraperitoneal injection of an overdose of ketamine (Taj Pharmaceuticals, Newcastle, UK)/xylasine (KHBoddin, Hamburg, Germany). The control animals were not treated with polyP or crushed aragonite, while the test animals received 150 mg polyP either alone or together with 150 mg crushed aragonite applied superficially into the open wound beds once, at day 0. Then the wounds were covered with Tegaderm transparent dressing (3M, St. Paul, MN, USA).

**Sample analysis: wound excision and morphometry.** The respective wound areas including the surrounding healthy tissue were excised post mortem and processed for histological assessment.[75] The slices were stained with hematoxylin–eosin.[76] The morphometric evaluation of the degree of re-epithelialization was performed optically with a Zeiss Axioskop (Zeiss, Oberkochen; Germany).

### 2.9. Microscopic analysis

The high resolution SEM images were taken with a Zeiss Gemini 1530 (Zeiss Oberkochem; Germany). For low resolution SEM studies an ESEM XL-30 machine (Philips, Eindhoven; Netherlands) was used. The samples were freeze-dried prior to inspection. In the SEM-ESEM experiments the samples were coated with gold.

### 2.10. Statistical analysis

For statistical analyses, the Student's *t* test or the Mann–Whitney *U*-test were applied. Accordingly, the GraphPad Prism 7.0 software (GraphPad, La Jolla, CA, USA) was used.

## 3. Results and discussion

### 3.1. Coacervation of crushed powdered pearls by polyP

The complex coacervate technology, based on interactions of oppositely charged polyelectrolytes in aqueous solution, has been successfully applied for drug delivery.[77–79] Formulations prepared by complex coacervation have the advantage that the active molecules are completely surrounded by the enveloping coacervate film. PolyP coacervates can be formed from polyP even in the presence of divalent cations such as $Ca^{2+}$.[18,19] The advantage of the polyP-based coacervate is that it is stable in a wide pH range from pH 5 (healthy individuals) to even the alkaline range with pH 8.[19] Covering the alkaline pH range is particularly important for the treatment of chronic wounds.[80,81] A further distinguished property of polyP is its high binding affinity to histidine-rich peptides, which control the organization of supramolecular biomaterials, especially those that bind to inorganic matrices,[82,83] implying that polyP-based coacervates are suitable for binding of aragonite calcareous nacre.

The finding that polyP and polyP coacervate cause a transformation of solid Ca-carbonate (crystalline aragonite) into a phase that is likewise soluble (Fig. 1) is used in nature to

 

self-assemble mineralic carbonate crystallites. This principle allows the formation of strong composite materials with filigree morphology, such as those used for construction of mollusk shells.[37] Conversely, in the present contribution the polyP polymer is used to re-convert the crystalline aragonite into a soluble phase. During this process, polyP acts as an anionic polymer, like the aspartic acid rich proteins in shells,[37] and as a platform for the phase transition of the crystalline aragonite plates.[84]

As thoroughly documented,[37,38,85] mussel shells are formed from crystalline aragonite, a metastable phase formed during the crystallization steps to stable calcite.[86] Exposure to polyP abolishes the thermodynamic "pump" mechanism and alters or even blocks phase transformation.[87,88] In addition, divalent cations such as $Mg^{2+}$ and certainly also $Ca^{2+}$ cause a change in the surface free energy and in turn the nucleation kinetics.[89]

As outlined in Fig. 1, co-incubation of pearl aragonite with polyP ends up in the formation of a coacervate, a process driven by Na-polyP and the subsequent $Ca^{2+}$ flux in the aqueous medium. The $Ca^{2+}$ ions shuttle between Ca-carbonate and the phosphate polymer in a non-enzymatic way.[90] As a result, polyP, together with $Ca^{2+}$ and carbonate, is converted into the biologically active coacervate phase, resulting in stimulation of the migratory ability of myofibroblasts, a key process in wound regeneration, especially of chronic wounds.[55,91]

The image of the inner shell abalone (Haliotis spec.) mollusc covered with an organic–inorganic nacreous, iridescent composite layer, is shown in Fig. 2(A)-a. In response to injury, pearls are formed below the Mantel and above the nacre layer (*H. schlegeli*/*H. cumingii*);[39] Fig. 2(A)-b and c.

**3.1.1. Characterization of the starting materials.** PolyP and aragonite (from nacre) were analyzed by both FTIR and XRD methods. The FTIR graphs of Na-polyP and Ca-polyP-NP show the characteristic signals for polyP with $\nu_{as}$(P–O–P) around a wavenumber of 902 $cm^{-1}$ and $\nu_s$(P–O–P) at 733 $cm^{-1}$. Marked are the signals at 1245 $cm^{-1}$, reflecting $\nu_{as}(PO_2)^-$ [the bridging phosphate], and at 1085 $cm^{-1}$, indicating $\nu_{as}(PO_3)^{2-}$, the terminal phosphate units (Fig. 2(B)).[92] These signals are also present in the polyP coacervate phase.[18] Furthermore, these characteristic signals are also visible in the coacervate obtained after addition of polyP in a weight ratio of 1 : 1 to aragonite (pearl powder) to wound exudate (Fig. 2(B)).

The Ca-polyP-NP are completely amorphous, as proven by the XRD diffractogram, which shows three smooth broad humps without any sharp diffraction peaks (Fig. 2(C)).[61] In contrast, the XRD aragonite (nacre) pattern shows the characteristic peaks and reflects the crystalline nature as described.[93]

**3.1.2. Coacervation of crushed powdered pearls initiated by Na-polyP.** Wound exudate has a composition similar to

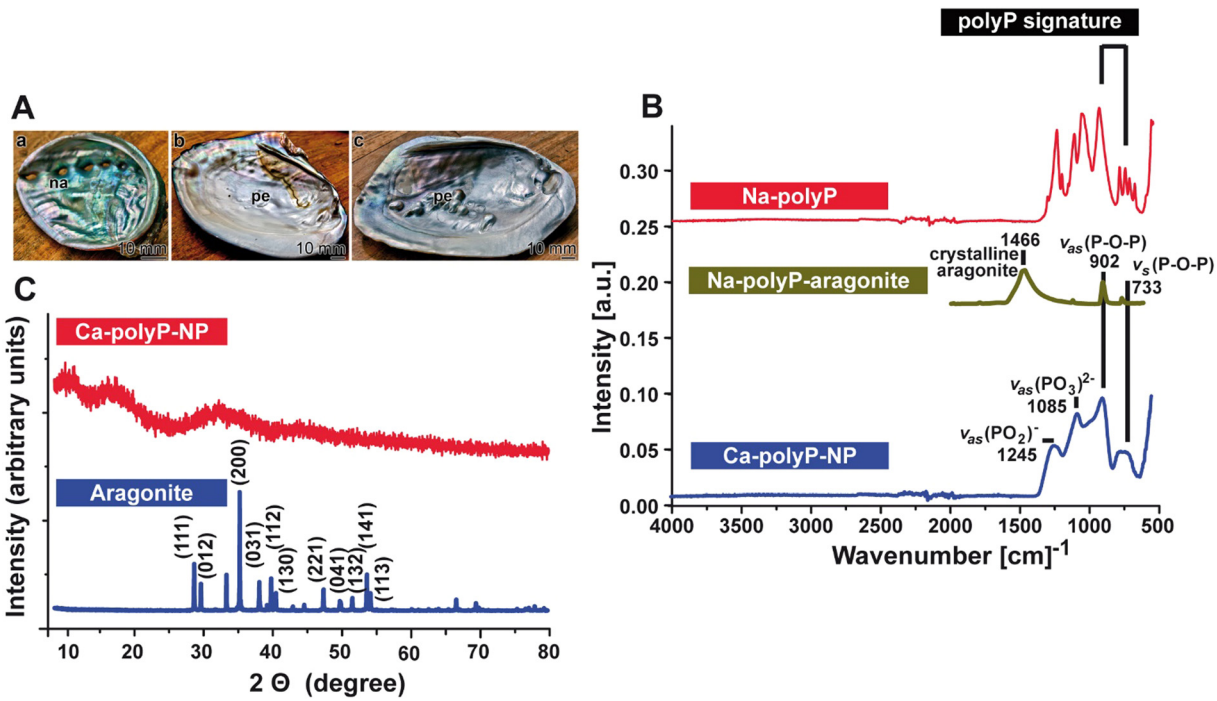


Fig. 2 Characterization of Na-polyP, Ca-polyP-NP and aragonite and of the coacervate formed from solid aragonite in presence of Na-polyP polyP by spectroscopical (FTIR) and X-ray diffraction (XRD) analysis. (A) Nacre (na) covering the inner side of bivalve shells produces pearls (pe) when injured. (a) Shell from Haliotis tuberculata with the nacre at the inner side. (b) and (c) Shells from *Hyriopsis schlegeli*/*Hyriopsis cumingii* with growing asymmetric pearls; after (b) 12 months or (c) 18 months of regeneration. (B) FTIR spectrum for polyP together with aragonite after reaching the coacervate phase (Na-polyP-aragonite) in comparison to the spectra of Na-polyP and Ca-polyP-NP. In the hybrid deposit (Na-polyP-aragonite in the coacervate form), the characteristic peaks for polyP and that for Ca-carbonate are visible. They are marked, the characteristic signatures for polyP (both for Na-polyP and Ca-polyP-NP) at 902 $cm^{-1}$ for $\nu_{as}$(P–O–P) and at 733 $cm^{-1}$ for $\nu_s$(P–O–P) as well as the peak at 1466 $cm^{-1}$ for aragonite. In addition, the signals at 1245 $cm^{-1}$ for the bridging phosphate $\nu_{as}(PO_2)^-$ and at 1085 $cm^{-1}$ for the terminal phosphate units $\nu_{as}(PO_3)^{2-}$ are marked. (C) XRD patterns of Ca-polyP-NP and aragonite. While the polyP graph diffractogram shows an amorphous halo, the aragonite graph matches aragonite.

serum and also contains $Ca^{2+}$;[94,95] the pH is around neutral.[96] As a result, this $Ca^{2+}$-rich environment allows rapid coacervation initiated by addition of Na-polyP (Fig. 3(I)).

Crushed powdered pearls with or without Na-polyP were suspended in either phosphate-buffered saline (PBS) or wound exudate at a final concentration 120 μg $mL^{-1}$ each. The suspension in PBS did not significantly change the irregular hexagonal crystal tablets that form the nacre pearls even after immersion for 3 h (Fig. 3(I)-A–C). The surfaces of the lamellae also retained their crystal morphology. In contrast, when the crystalline tablets were added to the wound exudate, the crystals began to dissolve after 3 h even in the absence of Na-polyP (Fig. 3(I)-D–F). Very pronounced is this process when the wound exudate is supplemented with Na-polyP (Fig. 3(I)-G–I). Dissolution started after an incubation of 1 h and was complete after 3 h. After this period, coacervate droplets with a size of ≈20 nm appeared (Fig. 3(I)-I).

**3.1.3. Coacervate formation of pearl crystals in wound exudate induced by Ca-polyP-NP.** The crushed pearl material retains its crystalline hexagonal tablet morphology in PBS (Fig. 3(II)-A–C). After transfer into the wound exudate supplemented with Ca-polyP-NP, an almost immediate dissolution of the aragonite sheets begins (Fig. 3(II)-D), which speeds up during a 1 h lasting incubation and, after 3 h, ends up in a homogeneous coacervate phase, which almost completely lacks the coacervate droplets (Fig. 3(II)-E and F).

**3.1.4. Coacervation of wound hydrogel supplemented with aragonite and polyP.** Wound care in a moist wound environment accelerates healing, reduces scarring, stimulates autolytic debridement and activates collagen synthesis.[97] The basis for the moisturizing solution are hydrogels or hydrocolloid-based oxygen dressings, which are assembled from colloidal particles or hydrophilic polymers and are dispersed in water.[98] Effective hydrogels should be biocompatible and mimic the natural extracellular matrix. Usually, synthetic hydrogels are applied, and, among those, cellulose derivatives-based dressings have been preferred for wound-healing.[99] In our patient-oriented application,[23] we introduced the semi-synthetic biopolymer hydroxyethyl cellulose as base material for the hydrogel. The problem with hydrogels for wound coverage is that they rapidly lose water unless the material is supplemented with ionic polymers. Furthermore, they are usually not stable.[98]

*3.1.4.1 Viscosity.* In the formulation tested on patients,[23] the hydroxyethyl cellulose-based hydrogel was supplemented with polyP (Na-polyP and Ca-polyP-NP), a composition that forms a stable coacervate (Fig. 3) in the presence body fluids such as wound exudate with its $Ca^{2+}$.[95] Importantly, the viscosity of the hydroxyethyl cellulose hydrogel increases after addition of polyP (100 μg $mL^{-1}$ of Na-polyP and 20 μg $mL^{-1}$ of Ca-polyP-NP) from 20 Pa s to 25 Pa s.[23] Further addition nacreous aragonite (120 μg $mL^{-1}$) to the mixture stabilized the hydrogel even further to a viscosity of 50 Pa s.

*3.1.4.2 Coacervate formation.* Injection of the hydrogel wound dressing supplemented with polyP and aragonite in PBS (containing only the monovalent cations $Na^+$ and $K^+$) does not result in bulging of the initial morphology of the roundish hydrogel drop (Fig. 4(I)-A and B). In contrast, if the hydrogel is injected into wound exudate, strong and distinct and time-dependent current flow patterns appear, which are typical for coacervate formation[23] (Fig. 4(I)-C–E). To demonstrate that $Ca^{2+}$, present in the wound exudate at ≈1.5 mM, is the causative component in the wound exudate that triggers

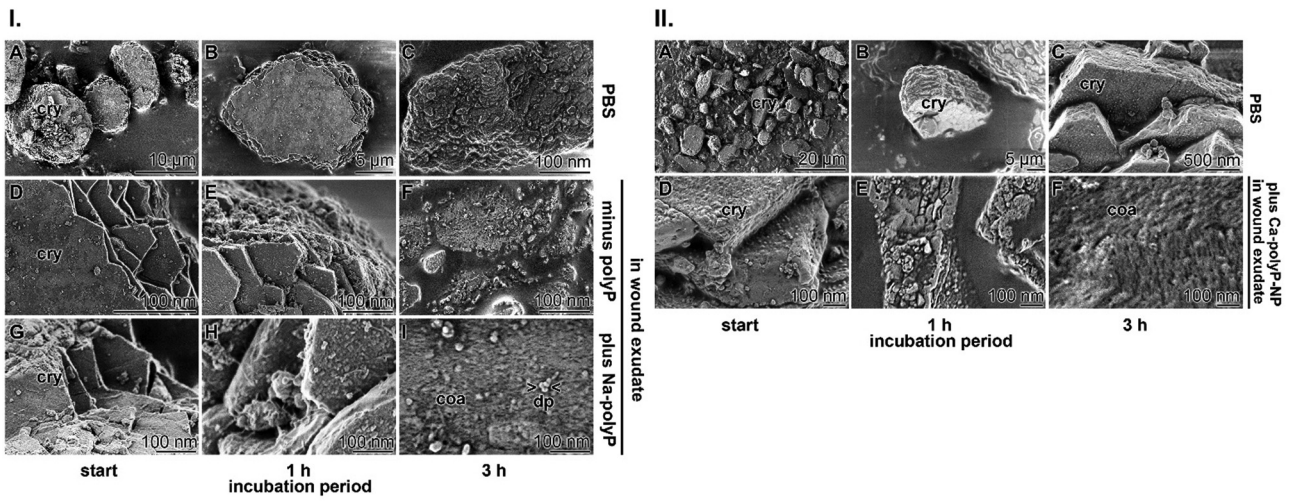


Fig. 3 Susceptibility of crystals from crushed powdered pearls to polyP. (I) When the tablets are immersed in PBS, the morphology of the (A) irregular hexagonal crystals (cry) does not change during an incubation period of (B) 1 h or (C) 3 h; also the surface texture remains unchanged. (D)–(F) However, when the crystals are immersed in wound exudate, the crystalline surfaces disintegrate, especially after 3 h. (G)–(I) Even more, when the wound exudate becomes supplemented with Na-polyP, the crystal pallets disintegrate completely, resulting in a coacervate with ≈20 nm sized coacervate (coa) droplets (dp). The respective incubation periods are given; SEM and ESEM. (II) Likewise, in the presence of Ca-polyP-NP, the crushed pearls also undergo phase transformation; SEM and ESEM. (A)–(C) Here too, when immersed in PBS, the crystal (cry) tablets keep their hexagonal shapes. (D)–(F) In contrast, when the crystals are immersed in the wound exudate together with Ca-polyP-NP, coacervation (coa) starts and ends with a complete phase transition.

 

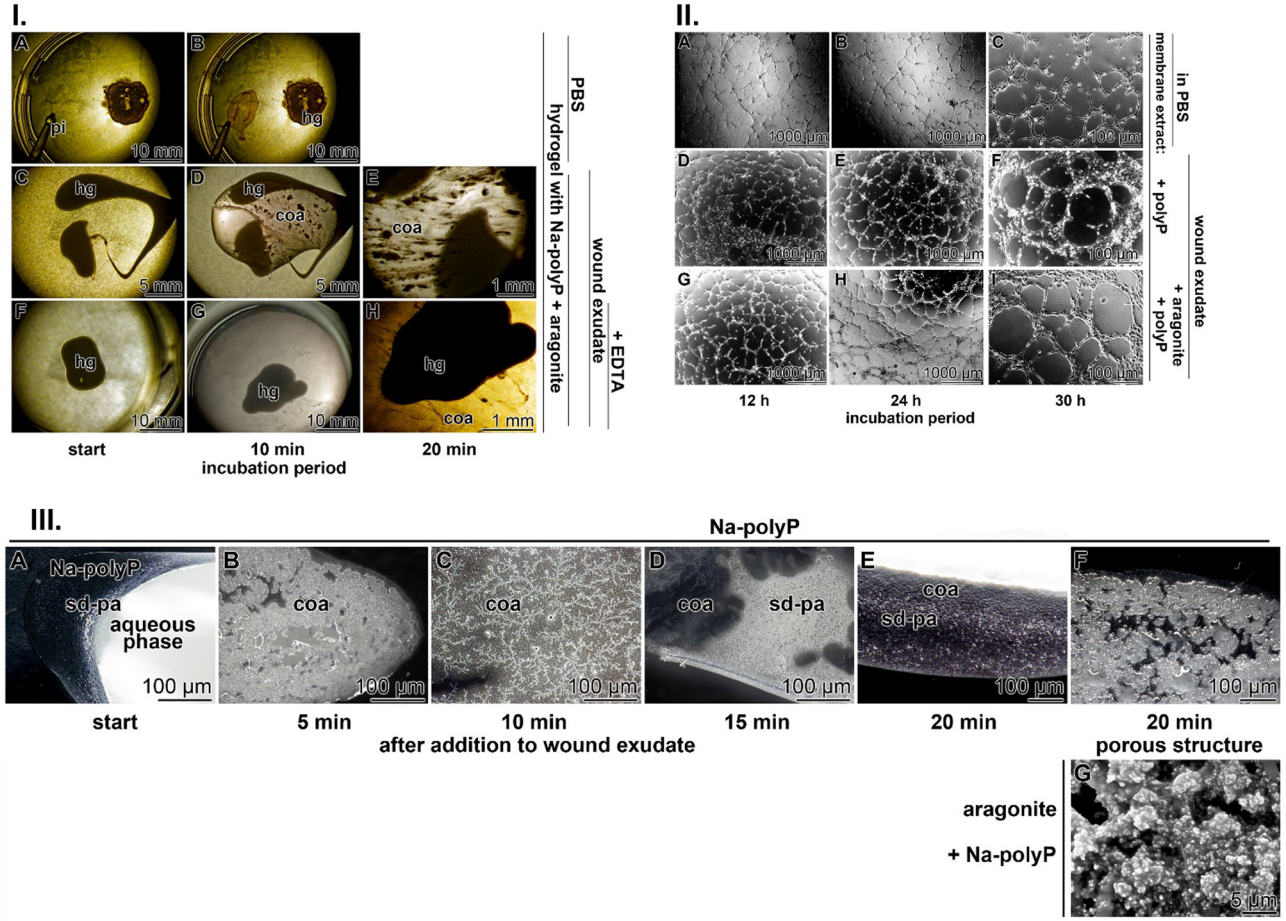


Fig. 4 Coacervate formation of the wound dressing hydrogel supplemented with polyP and aragonite in $Ca^{2+}$-free PBS or $Ca^{2+}$-containing wound exudate. (I) (A) and (B) Pipetting (pi) into PBS does not cause coacervation or even bulging of the initial roundish hydrogel (hg) drop. (C)–(E) Development of a current flow pattern reflecting coacervation after addition of the hydrogel filled with Na-polyP and aragonite into the $Ca^{2+}$-containing wound exudate. Already after an incubation period of 10 min, coacervate (coa) schlieren form, which increase in volume after 20 min. (F)–(H) When the wound exudate was preincubated with 1.5 mM $Na_2$-EDTA, the coacervate (coa) flow pattern is almost absent. (II) HUVEC monolayered tube formation (A)–(C) in assays overlaid on extracellular matrix material in PBS; SEM. When the matrix is (D)–(F) supplemented with the polyP cocktail, tube formation starts already between 12 h and 24 h after plating and is complete after 30 h of incubation. When the matrix is enriched (G)–(I) with both the polyP and the aragonite materials, monolayered tubes are formed already after 12 h and became steadily more pronounced. (III) Kinetics of coacervate formation in wound exudate; light microscopy. (A) After pipetting of 150 mg $mL^{-1}$ of Na-polyP into $Ca^{2+}$-rich wound exudate, the first small dense particles (sd-pa) appear, which act as nuclei for (B)–(D) denser coacervate (coa) deposits and then end up in extensive coacervate layers. The Na-polyP coacervate deposits show (F) a porous structure, which becomes more solidified (G) after inclusion of nacreous aragonite showing 5 μm sized pores.

coacervation, the wound fluid was supplemented with 1.5 mM $Na_2$–EDTA (ethylene–diamine–tetraacetic acid) in order to chelate divalent cations.[95,100] Under these conditions, coacervate formation is drastically suppressed (Fig. 4(I)-F–H)).

These data proved the concept sketched in Fig. 1 that polyP, particularly in the Na-polyP form, triggers a phase transition from crystalline nacreous aragonite to the amorphous phase. This transformation is based on the strong binding affinity of the divalent $Ca^{2+}$ cations to the anionic polymer. This interaction is accelerated by the property of Ca-polyP to be insoluble, which shifts the equilibrium towards destabilization of the crystalline state of aragonite. In the presence of an organic environment, the NP form of Ca-polyP undergoes coacervation and, concomitantly, also the nacreous aragonite, causing both deposits to turn into an aqueous phase. This reaction is the basis for the morphogenetic properties, with their inherent biological functions, of the two inorganic compounds.

**3.1.5. Kinetics of Na-polyP coacervation in wound exudate.** In a separate series of experiments, the kinetics of the Na-polyP-evoked coacervation process in wound exudate was studied (Fig. 4(III)). It is a rapid process. After pipetting a Na-polyP solution (150 mg $mL^{-1}$) into wound exudate containing $\approx$1.5 mM $Ca^{2+}$,[101] coacervate droplets are formed almost immediately (Fig. 4(III)-A). Within a period of 10 min, coacervate drops/flats are formed (Fig. 4(III)-B and C) which maturate into more solid coacervate fluffs (Fig. 4(III)-D) and end up with 100 μm to 300 μm coacervate layers (Fig. 4(III)-E). During this liquid–liquid phase separation, pores with a diameter of 40–50 μm are formed within the more solid polyP structure (Fig. 4(III)-F).

Importantly, after adding nacreous aragonite (150 μg $mL^{-1}$) to the Na-polyP solution at the beginning of the coacervation process, the more gelatinous structure of the gel is solidified, with pores around 5 μm, most likely stabilized by the remaining 1 μm large, cobble-like particles (Fig. 4(III)-G).

**Ethics.** Human wound exudate was collected in accordance with the rules of the declaration of Helsinki. In addition to these recommendations, the consent of the patients has been granted and the ethics committee of Rhineland-Palatinate gave its consent also [donated and approved by Hadrian Schepler (and the institutional committee of the Department of Dermatology, University Medical Center of the Johannes Gutenberg University, Langenbeckstraße 1, 55131 Mainz, GERMANY)].

### 3.2. Effect of soluble aragonitic Ca-carbonate on biological function

The coacervate, formed together with Na-polyP in the presence of $Ca^{2+}$ shows distinct biological activities.

**3.2.1. *In vitro* angiogenesis assay.** For the restauration and regeneration of chronic wound injuries, it is essential that new blood vessels sprout that supply the regenerating tissue with energy and growth factors.[29] More specifically, cells such as keratinocytes regulate the release of endogenous ATP during wound healing.[102] The release can occur both passively or actively, through cell lysis, vesicular exocytosis, pores or hemichannels.[103] These releases activate $P2Y_2$ receptors and stimulate PLC/$IP_3$ signaling, resulting in an increase in intracellular $Ca^{2+}$ followed by increased wound closure. Under impaired physiological conditions, ATP deficiency can be substituted by exogenous ATP packed into vesicles,[104] resulting in a stimulation of granulation tissue formation in parallel with collagen synthesis and neovascularization. Alternatively, polyP present in blood platelets has the potential to generate ATP by successive enzyme-mediated energy transfer during splitting of the high-energy acid anhydride phosphate bonds within the polymer driven by ALP and ADK.[12,105] Likewise, human studies also suggested that the platelet density is positively correlated with the ATP level in blood, while negatively correlated with the NADH level.[106] Even more, mitochondrial polyP can contribute to the cellular ATP pool.[107] In prokaryotes, ATP generation is accomplished by adenosine kinase coupled to polyphosphate kinases.[108]

A stimulatory effect on tube formation can be modeled *in vitro* by HUVEC endothelial cells embedded in extracellular matrix components.[109] In the studies summarized here, the matrix extract either remained nonsupplemented or was supplemented with either the polyP cocktail alone (Na-polyP and Ca-polyP-NP) or the mixture of polyP with the nacreous aragonite (Fig. 4(II)). In the controls without polyP and aragonite, the degree of tube formation was incomplete even after an incubation period of 30 h (Fig. 4(II)-A–C). In contrast, when the system was supplemented with the polyP cocktail alone, already after 12 h, the cells assumed a lobulated morphology and began to spread, forming distinct, although often incomplete, tube structures after 12 h, which became complete after 24 h and 30 h (Fig. 4(II)-D–F). Addition of polyP together with aragonite accelerated the tube-like pattern formation and most of the tube-like arrangements of the HUVEC cells were complete after 12 h and 24 h. Further extending the incubation to 30 h allowed the formation of cobblestones framing the tubes and smoothly arranged in monolayered rings (Fig. 4(II)-G–I).

**3.2.2. Enhanced gene expression of the vascularization biomarkers HIF-1α and VEGF in human HUVEC.** The cells were layered onto the wound dressing hydrogel after supplementation with polyP and aragonite in the $Ca^{2+}$-containing wound exudate under the same conditions used in the monolayered tube formation study. Immediately after seeding or after an incubation period of 12 h, 24 h or 30 h, the expression levels of the biomarkers HIF-1α and VEGF were quantitated by RT-qPCR (Fig. 5). After incubation for 12 h, a 35% increase in HIF-1α expression of the HUVEC is already measured, which doubles again after 24 h (Fig. 5). The kinetics of VEGF expression is slightly delayed, but increases to 245% after 24 h of incubation (Fig. 5).

**3.2.3. Increase in MSC proliferation.** MSC play a crucial role in all phases of wound healing, such as the inflammatory, proliferative, and remodelling stages.[110,111]

These cells were used to determine the effects of polyP and nacreous aragonite on the growth rate of cells. Incubation of MSC in the controls (with PBS) showed only a marginal increase in cell density under the conditions used compared to the positive potency of the polyP cocktail (Na-polyP and Ca-polyP-NP) and especially the polyP suspension together with nacreous aragonite (Fig. 6(I)). In all three series, with PBS (Fig. 6(I)-A and B), polyP cocktail (Fig. 6(I)-C and D) and with polyP together with nacreous aragonite (Fig. 6(I)-E and F) the densities of the MSC increased during the inspection period between the time of seeding and after 6 d of incubation.

Quantitative determination was possible by staining the cells with the cell viability reagent PrestoBlue (Fig. 6(II)).

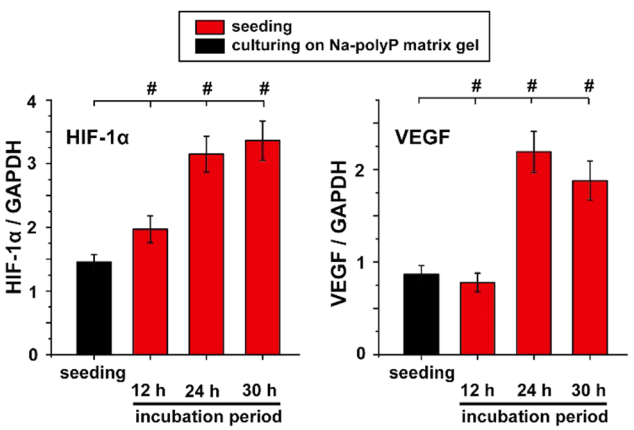


Fig. 5 Expression levels of HIF-1α and VEGF in HUVEC after incubation of the cells onto a layer of the wound dressing hydrogel, enriched with polyP and aragonite in the $Ca^{2+}$-containing wound exudate, as outlined in the *in vitro* angiogenesis assay. The steady-state expression levels were determined by RT-qPCR and are referred to the transcript levels of the housekeeping gene GAPDH. The results are means from 5 parallel experiments; $P < 0.01$; marked with #.

 

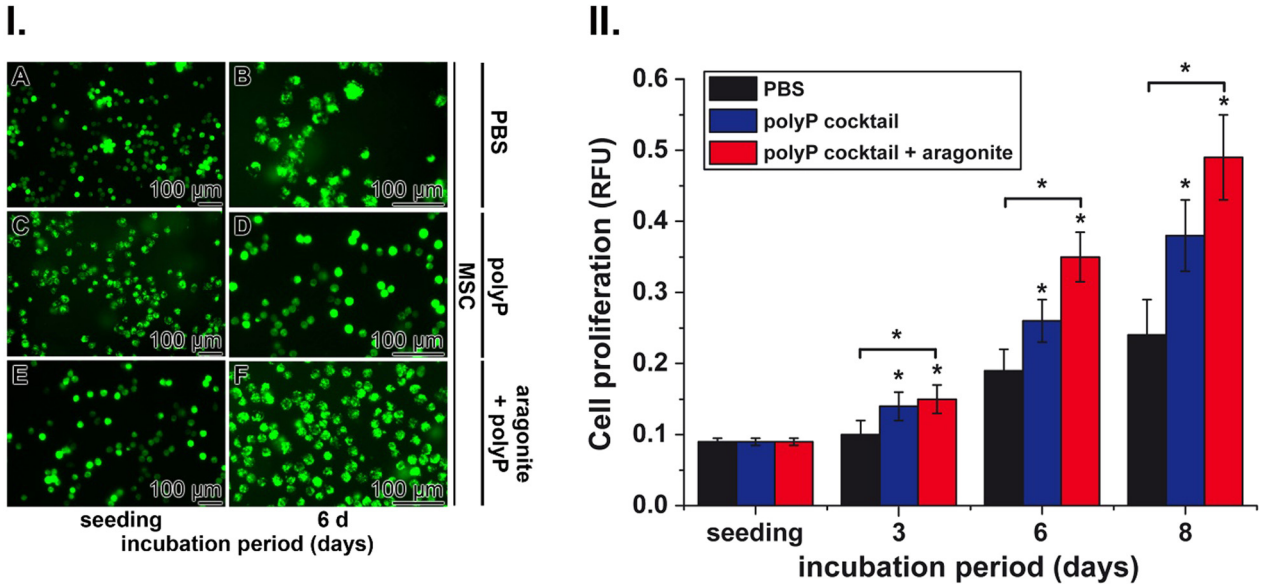


Fig. 6 Positive proliferation-stimulatory effect of polyP with nacreous aragonite on MSC. (I) MSC cultures were incubated with (A) and (B) PBS as a control or (C) and (D) a polyP cocktail (Na-polyP and Ca-polyP-NP) as well as with (E) and (F) the polyP cocktail, mixed with nacreous aragonite. The cultures supplemented with polyP and polyP plus aragonite grow to higher density compared to the controls after a 6 d incubation period; fluorescence light microscopy. (II) Quantitative determination of the proliferation-inducing effect with the viability reagent PrestoBlue. The MSC were incubated with either PBS (black bars), the polyP cocktail (blue bars), or with the polyP cocktail mixed with nacreous aragonite (red bars). The results are means ± SD from 10 parallel experiments (*$P < 0.01$).

In the PBS controls, the proliferation increased two-fold after an incubation period of 6 d and continued to ≈3-fold after 8 d of cultivation (Fig. 6(II)). The proliferation-inducing potency of polyP together with aragonite was significantly stronger compared to polyP alone and reached a 2-fold greater efficiency after an incubation period of 6 d and 8 d.

**3.2.4. Effect of wound hydrogel with its supplements on proliferation of MSC and bacteria.** It is the aim of a curative wound hydrogel to support regeneration, especially in chronic wounds, to support the growth of cells involved in tissue granulation and to prevent hyperproliferation of bacteria in the complex skin microbiota.[112,113] Since the bacteria of the skin microbiota contribute to immunological protection against invading pathogens, a careful antiseptic treatment of chronic wounds is indicated.[114,115]

Here, the effect of the wound hydrogel without or with polyP or polyP in combination with nacreous aragonite was tested using MSC as eukaryotic cell model and *Escherichia coli* M15 as bacterial system.

The MSC were added in the middle of the exponential growth phase to the wound exudate supplemented with the hydrogel either containing no polyP or supplemented with the polyP cocktail (Na-polyP and Ca-polyP-NP together with nacreous aragonite as outlined in the ''Experimental section''. After overnight incubation, the samples were fixed by freeze-drying and inspected by SEM and fluorescence microscopy (Fig. 7(A)–(H). The difference in cell morphology between the incubation series without and with polyP and aragonite is strong. In the absence of these additives the cells have a globular morphology (Fig. 7(A)–(D)), reflecting reduced cell–cell

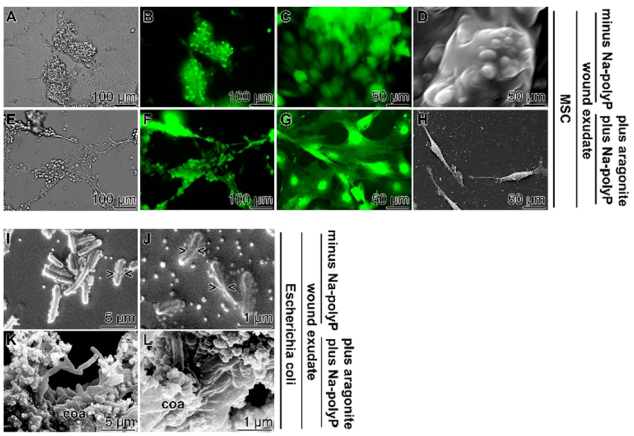


Fig. 7 Effect of polyP with aragonite on morphology of MSC and *E. coli* bacteria; SEM and fluorescence microscopy. The cultures were performed with 300 µL of culture medium plus 100 µL of hydrogel together with 100 µL of wound exudate. (A)–(H) MSC were embedded and, by this, exposed to hydrogel and wound exudate, which remained either (A)–(D) free of additional components or (E)–(H) was reacted with Na-polyP and nacreous aragonite. The black and white images (A) and (E) are taken with Nomarski optics; (D) and (H) are SEM images. The green fluorescent cells were stained with calcein AM. In contrast to the roundish morphology, the cells showing a spreading morphology are characterized by a strong overall cell metabolism. (I)–(L) Effect on bacteria (*E. coli*). No division structures (>·<) could be visualized in the assays with the coacervate (coa). Such constrictions can be seen in the control series, in which no coacervate is formed.

contact followed by reduced proliferation potency.[116] In contrast, MSC in cultures with polyP and aragonite spread vigorously and

often showed strong cell–cell contacts (Fig. 7(E)–(H)). This morphology is an indication for a viable cell metabolism.[117]

In a parallel series, *E. coli* M15 either remained unembedded (Fig. 7(I) and (J)) or were embedded in the polyP cocktail together with aragonite (Fig. 7(K) and (L)). In the latter polyP/aragonite assays, the bacterial cells were bricked in a coacervate. In this series, no signs of bacterial divisions were observed, whereas constrictions are present in the control series that does not develop a coacervate.

The antibacterial effect of the polyP cocktail together with aragonite was further demonstrated by determining the growth rate of *E. coli* in medium in the absence or presence of polyP and aragonite (Fig. 8). Already after a 3-h incubation period, the bacteria readily grow in the control (medium in the absence of the polyP/aragonite coacervate) to a density (at 600 nm) of $0.85 \pm 0.09$, while in the presence of the coacervate a density of $0.31 \pm 0.02$ was measured. The difference is even more distinct and significant after an incubation period of 10 h. At this stage, the density of the polyP/aragonite-treated cultures is only 20% of the rate reached in the polyP/aragonite-free control (Fig. 8).

**3.2.5. Polyphosphate as a driver of chronic wound regeneration.** The data summarized here show that polyP undergoes coacervation in the presence of wound exudate, containing the required $\approx$1.5 mM $Ca^{2+}$, and the wound hydrogel. The coacervation process is driven by a $Ca^{2+}$ flux and the process sequence is very rapid. Within this sequence, a transfer of the crystalline nacreous aragonite from the shells into the amorphous phase occurs. This Ca-carbonate constituent contributes significantly to the regeneratively active property of polyP, *e.g.* during tube formation, which mimics microvessel formation. In addition, polyP together with aragonite significantly stimulates the growth of MSC, which is also reflected by the change in the morphological phenotype of the cells from a rather more quiescent to a metabolically active, spreading phenotype, indicating an intense de- and repolymerization of actin filaments.[118]

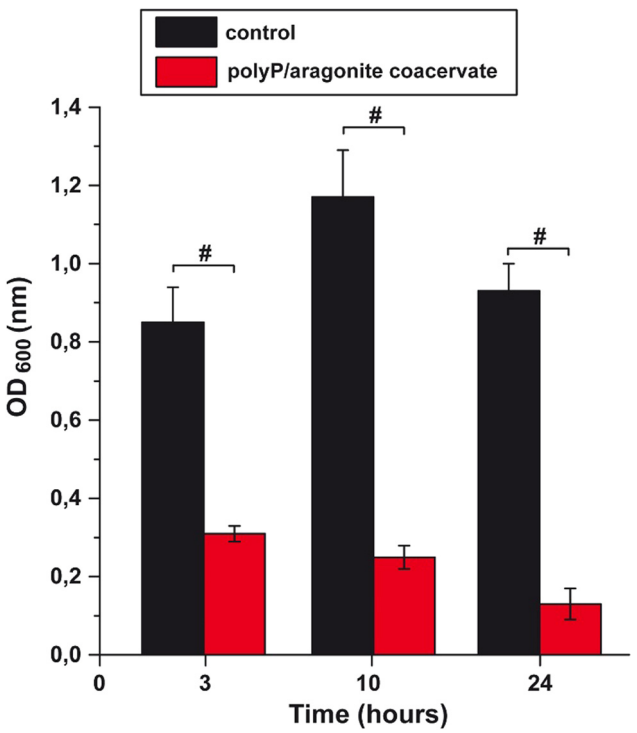


Fig. 8 Bacterial, *E. coli*, growth inhibition in medium supplemented with the polyP/aragonite coacervate. The data were calculated from five separate experiments; the corresponding mean values $\pm$ SDs are given as well. The significance/probability was calculated and is indicated ($P < 0.01$; #).

The rational explanation for the documented success of polyP in chronic wound healing is the transformation of polyP into its coacervate phase, as already concluded from *in vitro* studies.[18] Important, and documented here, is the result that this phase transition is driven by a liquid–liquid phase separation, initiated by $Ca^{2+}$, under formation of a thermodynamically reversible association between the oppositely charged ions, the polyanion polyP and the $Ca^{2+}$ cations.[20] During coacervation, the aqueous phase is squeezed out, resulting in a more porous, concentrated macromolecular structure.[119] The matrix of the gel-like, porous structure of the polyP coacervate becomes more stable through the inclusion of nacreous aragonite into the material. This property allows for a more efficient blood supply, particularly when this formulation is used to heal chronic wounds.

Based on the fact that wound healing is an energy-demanding process that requires both an extracellular ATP supply[19] and an intracellular ATP supply controlled by adenine nucleotide translocase-2 (ANT-2),[120,121] it was evident that polyP, especially Na-polyP, is an efficient component of the wound-healing hydrogel due to its coacervate-forming potency. While in healthy individuals skin injuries are restored within 2–3 weeks, this is different in diabetic patients. There, wounds fail to heal within about six months and can become chronic.[2] It is well documented that in chronic wounds the four different phases of wound healing, hemostasis, inflammation, proliferation and remodeling, are interrupted at one step or another. Frequently, a discontinuation of the healing process leads to persistent infections and peripheral vascular problems caused by an imbalance between angiogenic and angioinhibitory factors, which leads to disturbed regulation of angiogenesis.[122] Furthermore, and besides a disequilibrium of growth factors in the wound microenvironment, which also impairs balanced immune cell circulation, the lack of energy, a driving parameter in all phases of wound healing, is affected.[123] By this, the progress during the healing phases is blocked.

There are, in particular, infections of the wound that can result in an amputation of limbs.[124] Already here, Na-polyP has proven to achieve beneficial results.[23] In addition, it is reported here that bacteria become wrapped in the coacervate gel, preventing at least their overproliferation (Fig. 7). Moreover, an enhanced physiologic metabolism of eukaryotic MSC is observed. Considering these data, it appeared to be indicated to first investigate the effect of the Na-polyP-based wound-healing hydrogel in an animal study conducted on genetically engineered diabetic mice (db/db).[75] After that, a successful clinical proof-of-concept study has been undertaken.[23,29]

 

In order to find out whether the co-treatment of chronic wounds with Ca-polyP-NP and aragonite has an additional effect on wound healing compared to Ca-polyP-NP alone, an additional animal study was carried out using db/db mice, which show delayed wound healing. Experimental wounds (diameter 8 mm) were set in the interscapular region of the diabetic mice. The wounds were either left untreated or treated with either Ca-polyP-NP alone or with Ca-polyP-NP together with crushed aragonite, as described in the "Experimental section". The results showed that topical administration of polyP alone results in a significant reduction in wound diameter after a healing period of 7 d and 13 d compared to the untreated controls (Fig. 9), confirming previous results.[75] However, the effect of polyP on wound healing was significantly accelerated when the wounds were co-treated with Ca-polyP-NP and aragonite. After a healing period of 13 days, the diameter of the wounds treated with both components decreased to 78% of the wound diameter measured for Ca-polyP-NP alone and to 59% compared to wounds in the untreated animal group.

The dysregulation and imbalance of regeneration-promoting factors cause a reduction in angiogenesis, which is accompanied by a reduction of granulation tissue formation due to a nutrient and oxygen deficiency.[125] The granulation tissue is the decisive "germination" zone that develops after skin injury and from which the angiogenic processes take place, such as microvascular hyperpermeability, local degradation of the basement membrane, migration and sprouting of newly formed cells, giving rise to the formation of new blood vessels; finally, the reconstruction of the basement membrane occurs.[126]

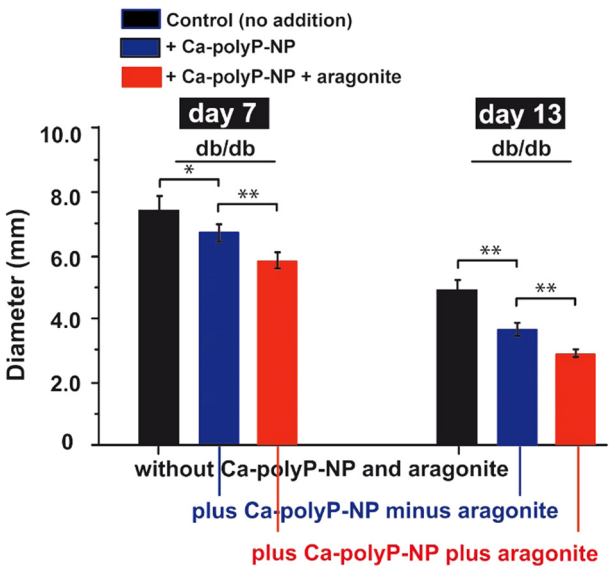


Fig. 9 Effect of polyP and polyP together with aragonite on healing of experimental wounds in diabetic db/db mice. Wounds were either left untreated or treated with Ca-polyP-NP alone or Ca-polyP-NP plus crushed aragonite as described in the "Experimental section". The wounds were examined at day 7 and day 13 and the diameters of the wounds (in mm) were determined. The data are presented as means ± SEM. Significances are $*P < 0.1$ and $**P < 0.05$; $n$ = 6–8 animals.

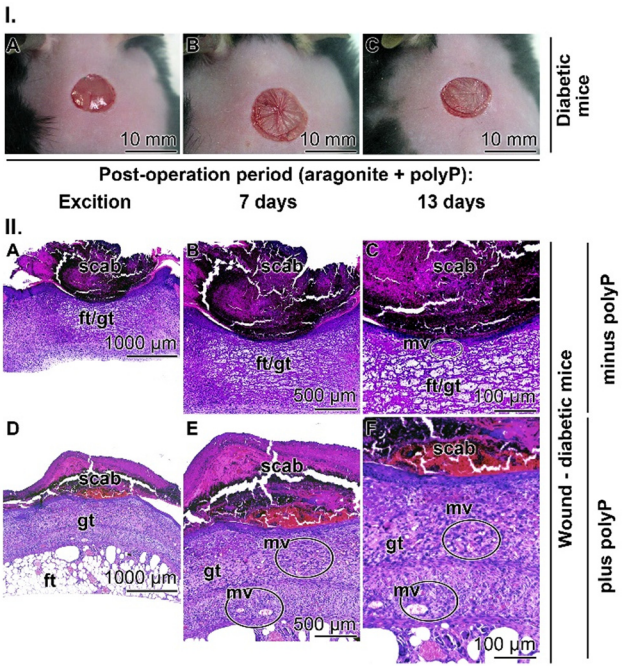


Fig. 10 Regeneration-inducing effect of polyP in the diabetic mice model. (I) After setting an excisional wound in the head/shoulder region along the dorsal midline, the wound was treated once with Ca-polyP-NP at the beginning of the healing period. After 7 d and 13 d, the formation of a granulation tissue started, but the surface scab is still present. The healing progress can only be clearly assessed after slicing the wound area and subsequent staining of the specimens with hematoxylin–eosin. (II) The slices obtained from wounds not treated with polyP (A)–(C) show below the scab only a thin layer with fat cells intermixed with granulating cells (ft/gt). Only rarely microvessels (mv) exist. (D)–(F) In contrast, in the section through the wound treated with Ca-polyP-NP, the granulation tissue (gt) is very massive and endothelial cells developed from stem cells are present that organize into microvessels (mv). The same histological section is displayed given at different magnifications to allow clear distinction of the different microvessel formation between the two treatment series.

To investigate the effects of Ca-polyP-NP on granulation tissue and microvessel formation, regenerating wounds of the db/db mice (Fig. 10(I)-A–C) were sliced and then stained with hematoxylin–eosin. In the diabetic control animals not treated with polyP, the regenerating wound was sealed with a scab, the hard, dried blood clot over the wound (Fig. 10(II)-A–C). The slices shown are taken from animals 13 d after setting the injury. In controls, not treated with polyP, the stained sections through the epidermis and the dermis show a voluminous hypodermis (connective tissue) composed of fat droplets. Basically, no granulation tissue can be discerned and therefore only very few microvessels are present. This histological observation fits well with previous findings reporting an increase in the fat layer within the connective tissue in diabetic patients.[127] Due to disturbed skin metabolism, diabetic patients often experience itchy and dry skin with the consequence that the patients are advised to apply skin-friendly cleansers and skin moisturizers.[128]

A completely different histological picture can be seen in tissues slices from diabetic mice treated with polyP (Fig. 10(II)-D–F)).

In these specimens it is immediately visible that the granulation tissue layer is very, very bulky, providing space and cell resources (endothelial cells) for extensive and dynamic microvessel development. From there, a controlled remodelling of the epidermis and dermis can start.[129]

## 4. Conclusion

It is an inherent property of coacervation that the microscale droplets formed during liquid–liquid phase separation are in a dynamic state, even during the apparent equilibrium of the phases. During this process, the liquid droplets are tightly packed together, influencing the interactions, free energy patterns and dynamic properties of the molecular constituents.[130] Liquid–liquid phase separations underlying aqueous two-phase systems are the basis for a number of biologically relevant processes, such as membrane biocondensation or supramolecular functional organization,[131] allowing complex biochemical reactions in a confined space.[132,133] In addition, they contribute to the understanding of the viscoelastic state of living organized systems.[134] Focusing on the topic here, liquid–liquid phase separation, coacervation, is also a key factor in wound healing,[135,136] in addition to the organization and migration of macrophages during tissue homeostasis, as well as the controlled supply of cytokines that suppress destructive immunity.[137] Even more, the development of those regulatory macrophages is promoted that trigger tissue remodeling and wound healing, including angiogenesis.[138]

The distinguished feature of the system reported here is that the previously published polyP-controlled coacervation, liquid–liquid phase separation, attracts MSC and activates them to actively migrate in the polyP coacervate matrix.[18] Coupled with the coacervation process of polyP is the effect of the polymer to attract and scavenge $Ca^{2+}$ from the labile crystalline aragonite phase and to include the carbonate anion into the dense phase of the formed Ca-polyP coacervate (Fig. 1). Vigorous flow areas certainly occur during the $Ca^{2+}$ flux as reported for $Ca^{2+}$/polyaspartate-rich coacervates.[139] In this microenvironment, upon separation of $Ca^{2+}$ from carbonate, a preferential surrounding for strong mineral deposition is found; calcium phosphate is formed at the expense of calcium carbonate. Even more, in the coacervate, continuous reactions (dynamic phase separations) occur that do not reach a thermodynamic equilibrium. Such nonequilibrium thermodynamics mimics biological systems, which are always in disequilibrium. Disequilibria between anabolic and catabolic reactions are the driving forces for biological systems.

Liquid–liquid phase separation processes, when broken down, are the onset of diseases such as amyloid formation in Alzheimer's disease. Direct exposure of neuronal cells to the amyloid-ß fragment Aß25-35 does not cause apoptosis; only after preincubation of the peptide for 5 d, cell toxicity can be seen.[140] Under physiological conditions, the cells exploit precautionary measures such as deaggregation caused by heat shock proteins that facilitate or prevent refolding.[141] Another driving force to keep the (bio)chemical reactions alive is ATP.[132,142] After enzymatic hydrolysis of the phosphoric acid anhydride bond in ATP, energy is released that is required for chemical bond formation or bond breakage in coupled reactions. Since ATP is formed after enzymatic hydrolysis of polyP,[12] especially in the extracellular environment, the results described in the present contribution adds two crucial aspects for stimulating regeneration processes in humans. First, the two interconnected coacervation circuits; Na-polyP with aragonite (Ca-carbonate) liquid–liquid phase separations and, second, ATP fueling for the regenerating areas as long as polyP is present at the repair site. It is the dynamics of the bicomponent liquid–liquid phase separation/coacervation system that accelerates wound regeneration by the present formulation, including tube formation and increased MSC proliferation as shown here or proposed based on the asymmetric cluster vibrations provoked by intrinsic non-isotropic ATP consumption.[143]

Future experiments will follow to contribute to the understanding of the bicomponent coacervation reported here in other aspects of skin disorders, such as thermoregulatory sweating during hypohidrosis or anhidrosis, which is likewise primarily due to an impaired ATP homeostasis, based on dysfunction of Na,K-ATPase activity.[144] Other promising potential applications would be psoriasis, a disease related to wound healing[145] and characterized by a switch of keratinocytes from growth to differentiation due to a dysregulation of *N*-methyl-D-aspartate receptor (NMDAR) in these cells. Since memantine is a blocker of NMDAR,[146] a curative approach could be the encapsulation of this drug in polyP-based core–shell NP.[147]

## Author contributions

Werner E. G. Müller: conceptualization, data curation, formal analysis, original draft, writing – review and editing. Meik Neufurth: methodology, writing. Xiaohong Wang: data curation, writing, investigation, strategic focus. Shunfeng Wang: data curation, methodology, nanoparticle preparation, coacervation studies. Hadrian Schepler: human studies; histology. Rafael Muñoz-Espí: spectroscopic methodology, data analysis. Hiroshi Ushijima: data curation, writing of methods. Heinz C. Schröder: conceptualization, discussion, corrections, supervisions.

## Data availability

The data that support the findings of this study are available on request from the corresponding author, upon reasonable request.

## Conflicts of interest

The authors declare no competing interest.

 

## Acknowledgements

We thank Prof. Dr Vesna Erakovic Haber and Dr Dinko Relkovic (both at Fidelta Ltd., Zagreb; Croatia) for important contributions with the animal wound healing studies during the EU integrated project BlueGenics (grant no. 311848; 2012–2016). Furthermore we appreciate the contributions of Ms Kerstin Bahr, Institute of Functional and Clinical Anatomy, University Medical Center of the Johannes Gutenberg University, Mainz (Germany) for continuous support. Finally, we sincerely express our thanks to Mr Gunnar Glasser (Department of Physical Chemistry of Polymers, Max Planck Institute for Polymer Research, Mainz; Germany) for continuous and very expert support for the SEM analyses. W. E. G. M. is the holder of an ERC Advanced Investigator Grant (grant number 268476). In addition, W. E. G. M. has obtained three ERC-PoC grants (Si-Bone-PoC, grant no. 324564; MorphoVES-PoC, grant no. 662486; and ArthroDUR, grant no. 767234). Further support came from the BMBF (Chinese-German cooperation in industry-led collaborative project "SKIN-ENERGY" – FKZ 13GW0403B). Finally, this work was supported by grants from the International Human Frontier Science Program and the BiomaTiCS research initiative of the University Medical Center, Mainz.

## References

1 N. M. Vecin and R. S. Kirsner, *Front. Med.*, 2023, **10**, 1154567.
2 A. J. Singer and R. A. Clark, *N. Engl. J. Med.*, 1999, **341**, 738–746.
3 A. V. Nguyen and A. M. Soulika, *Int. J. Mol. Sci.*, 2019, **20**, 1811.
4 A. Sreedhar, L. Aguilera-Aguirre and K. K. Singh, *Cell Death Dis.*, 2020, **11**, 444.
5 F. Lipman, *Adv. Enzymol. Relat. Subj. Biochem.*, 1941, **1**, 99–162.
6 A. Trautmann, *Sci. Signaling*, 2009, **26**, pe6.
7 L. L. Feng, Y. Q. Cai, M. C. Zhu, L. J. Xing and X. Wang, *Cancer Cell Int.*, 2020, **20**, 110.
8 *Inorganic Polyphosphates – Biochemistry, Biology, Biotechnology*, ed. H. C. Schröder and W. E. G. Müller, Springer Press, Heidelberg, 1999.
9 I. S. Kulaev, V. Vagabov and T. Kulakovskaya, *The Biochemistry of Inorganic Polyphosphates*, John Wiley, Chichester, 2004.
10 N. N. Rao, M. R. Gómez-García and A. Kornberg, *Annu. Rev. Biochem.*, 2009, **78**, 605–647.
11 T. L. Lindahl, S. Ramström, N. Boknäs and L. Faxälv, *Biochem. Soc. Trans.*, 2016, **44**, 35–39.
12 W. E. G. Müller, H. C. Schröder and X. H. Wang, *Chem. Rev.*, 2019, **119**, 12337–12374.
13 H. Holmsen and H. J. Weiss, *Annu. Rev. Med.*, 1979, **30**, 119–134.
14 M. H. Fukami, C. A. Dangelmaier, J. S. Bauer and H. Holmsen, *Biochem. J.*, 1980, **192**, 99–105.
15 W. E. G. Müller, S. F. Wang, M. Neufurth, M. Kokkinopoulou, Q. L. Feng, H. C. Schröder and X. H. Wang, *J. Cell Sci.*, 2017, **130**, 2747–2756.
16 Y. Akosah, J. Yang and E. Pavlov, *Biochem. Soc. Trans.*, 2024, **52**, 671–679.
17 A. Y. Baev, P. R. Angelova and A. Y. Abramov, *Biochem. J.*, 2020, **477**, 1515–1524.
18 W. E. G. Müller, E. Tolba, M. Neufurth, M. Ackermann, R. Muñoz-Espí, I. Lieberwirth, G. Glasser, H. C. Schröder and X. H. Wang, *Small*, 2018, **14**, 1801170.
19 W. E. G. Müller, M. Neufurth, I. Lieberwirth, S. F. Wang, H. C. Schröder and X. H. Wang, *Mater. Today Bio*, 2022, **16**, 100404.
20 D. W. R. Balkenende, S. M. Winkler and P. B. Messersmith, *Eur. Polym. J.*, 2019, **116**, 134–143.
21 A. N. Singh and A. Yethiraj, *J. Phys. Chem. B*, 2021, **125**, 3023–3031.
22 S. Chen, Q. Guo and J. Yu, *Aggregate*, 2022, **3**, e293.
23 W. E. G. Müller, H. Schepler, M. Neufurth, S. F. Wang, V. Ferrucci, M. Zollo, R. W. Tan, H. C. Schröder and X. H. Wang, *J. Mater. Sci. Technol.*, 2023, **135**, 170–185.
24 E. Tolba, W. E. G. Müller, B. M. A. El-Hady, M. Neufurth, F. Wurm, S. F. Wang, H. C. Schröder and X. H. Wang, *J. Mater. Chem. B*, 2016, **4**, 376–386.
25 X. Li, X. Yang, X. Liu, W. He, Q. Huang, S. Li and Q. Feng, *Prog. Nat. Sci.: Mater. Int.*, 2018, **28**, 598–608.
26 X. H. Wang, H. C. Schröder and W. E. G. Müller, *J. Mater. Chem. B*, 2018, **6**, 2385–2412.
27 W. E. G. Müller, M. Neufurth, S. F. Wang, H. C. Schröder and X. H. Wang, *Small*, 2024, 2309528.
28 Y. Wang, M. Li, P. Li, H. Teng, D. Fan, W. Du and Z. Guo, *BioMed Res. Int.*, 2019, **2019**, 5141204.
29 H. Schepler, M. Neufurth, S. F. Wang, Z. She, H. C. Schröder, X. H. Wang and W. E. G. Müller, *Theranostics*, 2022, **12**, 18–34.
30 A. M. Moe, A. E. Golding and W. M. Bement, *Semin. Cell Dev. Biol.*, 2015, **45**, 18–23.
31 S. F. Wang, M. Neufurth, H. Schepler, R. Tan, Z. She, B. Al-Nawas, X. H. Wang, H. C. Schröder and W. E. G. Müller, *Pharmaceutics*, 2023, **15**, 494.
32 C. Navarro-Requena, S. Pérez-Amodio, O. Castaño and E. Engel, *Nanotechnology*, 2018, **29**, 395102.
33 T. Subramaniam, M. B. Fauzi, Y. Lokanathan and J. X. Law, *Int. J. Mol. Sci.*, 2021, **22**, 6486.
34 J. Liang, D. Kang, Y. Wang, Y. Yu, J. Fan and E. Takashi, *PLoS One*, 2015, **10**, e0117106.
35 O. Sulpis, E. Jeansson, A. Dinauer and S. K. Lauvset, *Nat. Geosci.*, 2021, **14**, 423–428.
36 V. Lauth, M. Maas and K. Rezwan, *J. Mater. Chem. B*, 2014, **2**, 7725–7731.
37 L. Addadi, D. Joester, F. Nudelman and S. Weiner, *Chemistry*, 2006, **12**, 980–987.
38 L. Qiao, Q. L. Feng and S. Lu, *Cryst. Growth Des.*, 2008, **8**, 1509–1514.
39 J. Sun and B. Bhushan, *RSC Adv.*, 2012, **2**, 7617–7632.

40 J. Pei, Y. Wang, X. Zou, H. Ruan, C. Tang, J. Liao, G. Si and P. Sun, *Front. Bioeng. Biotechnol.*, 2021, **9**, 649665.
41 C. A. Schmidt, E. Tambutté, A. A. Venn, Z. Zou, C. Castillo Alvarez, L. S. Devriendt, H. A. Bechtel, C. A. Stifler, S. Anglemyer, C. P. Breit, C. L. Foust, A. Hopanchuk, C. N. Klaus, I. J. Kohler, I. M. LeCloux, J. Mezera, M. R. Patton, A. Purisch, V. Quach, J. S. Sengkhammee and P. U. P. A. Gilbert, *Nat. Commun.*, 2024, **15**, 1812.
42 F. Vallés, *Controversiarum Medicarum et Philosophicarum libri decem*, Marnius & Aubrius, Hanoviae, 1606, p. 368.
43 X. J. Loh, D. J. Young, H. Guo, L. Tang, Y. Wu, G. Zhang, C. Tang and H. Ruan, *Materials*, 2021, **14**, 2797.
44 M. Liu, J. Tao, H. Guo, L. Tang, G. Zhang, C. Tang, H. Zhou, Y. Wu, H. Ruan and X. J. Loh, *Materials*, 2021, **14**, 4458.
45 E. Lopez, A. Le Faou, S. Borzeix and S. Berland, *Tissue Cell*, 2000, **32**, 95–101.
46 D. W. Green, H. J. Kwon and H. S. Jung, *Mol. Cells*, 2015, **38**, 267–272.
47 F. Müller, N. J. Mutch, W. A. Schenk, S. A. Smith, L. Esterl, H. M. Spronk, S. Schmidbauer, W. A. Gahl, J. H. Morrissey and T. Renné, *Cell*, 2009, **139**, 1143–1156.
48 L. Faxälv, N. Boknäs, J. O. Ström, P. Tengvall, E. Theodorsson, S. Ramström and T. L. Lindahl, *Blood*, 2013, **122**, 3818–3824.
49 B. Lorenz and H. C. Schröder, *Biochim. Biophys. Acta*, 2001, **1547**, 254–261.
50 S. A. Smith, S. H. Choi, R. Davis-Harrison, J. Huyck, J. Boettcher, C. M. Rienstra and J. H. Morrissey, *Blood*, 2011, **117**, 3477.
51 J. J. Verhoef, A. D. Barendrecht, K. F. Nickel, K. Dijkxhoorn, E. Kenne, L. Labberton, O. J. McCarty, R. Schiffelers, H. F. Heijnen, A. P. Hendrickx, H. Schellekens, M. H. Fens, S. de Maat, T. Renné and C. Maas, *Blood*, 2017, **129**, 1707–1717.
52 W. L. Dean, *World J. Biol. Chem.*, 2010, **1**, 265–270.
53 R. Docampo and S. N. Moreno, *Cell Calcium*, 2011, **50**, 113–119.
54 S. Omelon, A. Baer, T. Coyle, R. M. Pilliar, R. Kandel and M. Grynpas, *Mater. Res. Bull.*, 2008, **43**, 68–80.
55 Y. C. Li, C. R. Chen and T. H. Young, *Pharm. Biol.*, 2013, **51**, 289–297.
56 L. M. Harwood, L. C. Hodgkinson, J. K. Sutherland and P. Towers, *Can. J. Chem.*, 1984, **62**, 1922–1925.
57 V. P. Kutyshenko, M. Molchanov, P. Beskaravayny, V. N. Uversky and M. A. Timchenko, *PLoS One*, 2011, **6**, e28824.
58 N. Ferrara, *Oncologist*, 2004, **9**(Suppl. 1), 2–10.
59 Y. Zhang, Y. Xu, J. Ma, X. Pang and M. Dong, *Sci. Rep.*, 2017, **7**, 40524.
60 J. Gim, A. Koch, L. M. Otter, B. H. Savitzky, S. Erland, L. A. Estroff, D. E. Jacob and R. Hovden, *Proc. Natl. Acad. Sci. U. S. A.*, 2021, **118**, e2107477118.
61 W. E. G. Müller, E. Tolba, H. C. Schröder, S. F. Wang, G. Glaßer, R. Muñoz-Espí, T. Link and X. H. Wang, *Mater. Lett.*, 2015, **148**, 166.
62 W. E. G. Müller, M. Ackermann, S. F. Wang, M. Neufurth, R. Muñoz-Espí, Q. L. Feng, H. C. Schröder and X. H. Wang, *Cell. Mol. Life Sci.*, 2018, **75**, 21–32.
63 D. Xie, D. Ju, C. Speyer, D. Gorski and M. A. Kosir, *J. Visualized Exp.*, 2016, **114**, e54074.
64 M. Neufurth, S. F. Wang, H. C. Schröder, B. Al-Nawas, X. H. Wang and W. E. G. Müller, *Biofabrication*, 2022, **14**, 015016.
65 W. E. G. Müller, M. Neufurth, S. F. Wang, H. C. Schröder and X. H. Wang, *Cancers*, 2021, **13**, 750.
66 M. Xu, D. J. McCanna and J. G. Sivak, *J. Pharmacol. Toxicol. Methods*, 2015, **71**, 1–7.
67 W. E. G. Müller, S. Engel, X. H. Wang, S. E. Wolf, W. Tremel, N. L. Thakur, A. Krasko, M. Divekar and H. C. Schröder, *Biomaterials*, 2008, **29**, 771–779.
68 A. Giacomini, M. Ackermann, M. Belleri, D. Coltrini, B. Nico, D. Ribatti, M. A. Konerding, M. Presta and M. Righi, *Angiogenesis*, 2015, **18**, 499–510.
69 J. Campbell, *Curr. Protoc. Chem. Biol.*, 2011, **3**, 100115.
70 M. Wiens, X. H. Wang, U. Schloßmacher, I. Lieberwirth, G. Glasser, H. Ushijima, H. C. Schröder and W. E. G. Müller, *Calcif. Tissue Int.*, 2010, **87**, 513–524.
71 M. Wiens, X. H. Wang, H. C. Schröder, U. Kolb, U. Schloßmacher, H. Ushijima and W. E. G. Müller, *Biomaterials*, 2010, **31**, 7716–7725.
72 S. M. Manohar, A. A. Padgaonkar, A. Jalota-Badhwar, V. Sonawane, M. J. Rathos, S. Kumar and K. S. Joshi, *BMC Cancer*, 2011, **11**, 338.
73 R. D. Barber, D. W. Harmer, R. A. Coleman and B. J. Clark, *Physiol. Genomics*, 2005, **21**, 389–395.
74 M. W. Pfaffl, *Nucleic Acids Res.*, 2001, **29**, 2002–2007.
75 W. E. G. Müller, D. Relkovic, M. Ackermann, S. F. Wang, M. Neufurth, A. Paravic-Radicevic, H. Ushijima, H. C. Schröder and X. H. Wang, *Polymers*, 2017, **9**, 300.
76 R. D. Lillie, *Histopathologic Technic and Practical Histochemistry*, McGraw-Hill Book Co., New York, USA, 3rd edn, 1965.
77 S. van der Burgh, A. de Keizer and M. A. Stuart, *Langmuir*, 2004, **20**, 1073–1084.
78 E. Ortega-Rivas, P. Juliano and H. Yan, *Food powders: Physical properties, processing, and functionality*, Springer Science & Business Media, New York, 2006.
79 Y. P. Timilsena, T. O. Akanbi, N. Khalid, B. Adhikari and C. J. Barrow, *Int. J. Biol. Macromol.*, 2019, **121**, 1276–1286.
80 T. R. Dargaville, B. L. Farrugia, J. A. Broadbent, S. Pace, Z. Upton and N. H. Voelcker, *Biosens. Bioelectron.*, 2013, **41**, 30–42.
81 H. H. Leveen, G. Falk, B. Borek, C. Diaz, Y. Lynfield, B. J. Wynkoop, G. A. Mabunda, J. L. Rubricius and G. C. Christoudias, *Ann. Surg.*, 1973, **178**, 745–753.
82 Y. Chen, K. Tao, W. Ji, V. B. Kumar, S. Rencus-Lazar and E. Gazit, *Mater. Today*, 2022, **60**, 106–127.
83 N. Neville, K. Lehotsky, Z. Yang, K. A. Klupt, A. Denoncourt, M. Downey and Z. Jia, *Cell Rep.*, 2023, **42**, 113082.
84 J. H. E. Cartwright, A. G. Checa and C. I. Sainz-Díaz, *ACS Nano*, 2020, **14**, 9277–9281.
85 L. E. Murr and D. A. Ramirez, *JOM*, 2012, **64**, 469–474.
86 L. A. Casella, E. Griesshaber, X. Yin, A. Ziegler, V. Mavromatis, D. Müller, A. C. Ritter, D. Hippler, E. M. Harper and M. Dietzel, *Biogeosciences*, 2017, **14**, 1461–1492.

87 B. Gao and K. M. Poduska, *Solids*, 2022, **3**, 684–696.
88 B. Gao, K. M. Poduska, S. Kababya and A. Schmidt, *J. Am. Chem. Soc.*, 2023, **145**, 25938–25941.
89 K. J. Davis, P. M. Dove and J. J. De Yoreo, *Science*, 2000, **290**, 1134–1137.
90 W. E. G. Müller, M. Neufurth, J. Huang, K. Wang, Q. L. Feng, H. C. Schröder, B. Diehl-Seifert, R. Muñoz-Espí and X. H. Wang, *ChemBioChem*, 2015, **16**, 1323–1332.
91 B. Hinz, *Curr. Res. Transl. Med.*, 2016, **64**, 171–177.
92 A. Khoshmanesh, P. L. Cook and B. R. Wood, *Analyst*, 2012, **137**, 3704–3709.
93 C. G. Kontoyannis and N. V. Vagenas, *Analyst*, 2000, **125**, 251–255.
94 I. R. Sweeney, M. Miraftab and G. Collyer, *Int. Wound J.*, 2012, **9**, 601–612.
95 T. Subramaniam, M. B. Fauzi, Y. Lokanathan and J. X. Law, *Int. J. Mol. Sci.*, 2021, **22**, 6486.
96 V. K. Shukla, D. Shukla, S. K. Tiwary, S. Agrawal and A. Rastogi, *J. Wound Care*, 2007, **16**, 291–294.
97 J. Harvey, K. T. Mellody, N. Cullum, R. E. B. Watson and J. Dumville, *Wound Repair Regen.*, 2022, **30**, 317–333.
98 B. J. Tighe and A. Mann, in *Woodhead Publishing Series in Biomaterials – Advanced Wound Repair Therapies*, ed. D. Farrar, Elsevier, Ansterdam, 2011, pp. 321–357.
99 E. E. Tudoroiu, C. E. Dinu-Pirvu, M. G. Albu Kaya, L. Popa, V. Anuta, R. M. Prisada and M. V. Ghica, *Pharmaceuticals*, 2021, **14**, 1215.
100 H. Hennings, D. Michael, C. Cheng, P. Steinert, K. Holbrook and S. H. Yuspa, *Cell*, 1980, **19**, 245–254.
101 J. J. Grzesiak and M. D. Pierschbacher, *J. Clin. Invest.*, 1995, **95**, 227–233.
102 T. B. McEwan, R. A. Sophocleous, P. Cuthbertson, K. J. Mansfield, M. L. Sanderson-Smith and R. Sluyter, *Life Sci.*, 2021, **283**, 119850.
103 M. Dosch, J. Gerber, F. Jebbawi and G. Beldi, *Int. J. Mol. Sci.*, 2018, **19**, 1222.
104 Y. Mo, H. Sarojini, R. Wan, Q. Zhang, J. Wang, S. Eichenberger, G. J. Kotwal and S. Chien, *Front. Pharmacol.*, 2020, **10**, 1502.
105 W. E. G. Müller, E. Tolba, Q. L. Feng, H. C. Schröder, J. S. Markl, M. Kokkinopoulou and X. H. Wang, *J. Cell Sci.*, 2015, **128**, 2202–2207.
106 T. Ushiki, T. Mochizuki, K. Suzuki, M. Kamimura, H. Ishiguro, T. Suwabe and T. Kawase, *Int. J. Mol. Sci.*, 2022, **23**, 11293.
107 M. Guitart-Mampel, P. Urquiza, F. Carnevale Neto, J. R. Anderson, V. Hambardikar, E. R. Scoma, G. E. Merrihew, L. Wang, M. J. MacCoss, D. Raftery, M. J. Peffers and M. E. Solesio, *Front. Cell Dev. Biol.*, 2022, **10**, 833127.
108 B. Nocek, S. Kochinyan, M. Proudfoot, G. Brown, E. Evdokimova, J. Osipiuk, A. M. Edwards, A. Savchenko, A. Joachimiak and A. F. Yakunin, *Proc. Natl. Acad. Sci. U. S. A.*, 2008, **105**, 17730–17735.
109 A. M. Goodwin, *Microvasc. Res.*, 2007, **74**, 172–183.
110 M. Rodrigues, N. Kosaric, C. A. Bonham and G. C. Gurtner, *Physiol. Rev.*, 2019, **99**, 665–706.
111 S. Maxson, E. A. Lopez, D. Yoo, A. Danilkovitch-Miagkova and M. A. Leroux, *Stem Cells Transl. Med.*, 2012, **1**, 142–149.
112 A. L. Byrd, Y. Belkaid and J. A. Segre, *Nat. Rev. Microbiol.*, 2018, **16**, 143–155.
113 S. Carmona-Cruz, L. Orozco-Covarrubias and M. Sáez-de-Ocariz, *Front. Cell. Infect. Microbiol.*, 2022, **12**, 834135.
114 J. D. Rembe, C. Fromm-Dornieden, J. Böhm and E. K. Stuermer, *Wound Repair Regen.*, 2018, **26**, 27–35.
115 J. Roewe, G. Stavrides, M. Strueve, A. Sharma, F. Marini, A. Mann, S. A. Smith, Z. Kaya, B. Strobl, M. Mueller, C. Reinhardt, J. H. Morrissey and M. Bosmann, *Nat. Commun.*, 2020, **11**, 4035.
116 J. P. Woodley, D. W. Lambert and I. O. Asencio, *Tissue Eng., Part B*, 2022, **28**, 569–578.
117 R. L. Splitt and K. A. DeMali, *Biol. Cell.*, 2023, **115**, e202200108.
118 M. A. Fardin, O. M. Rossier, P. Rangamani, P. D. Avigan, N. C. Gauthier, W. Vonnegut, A. Mathur, J. Hone, R. Iyengar and M. P. Sheetz, *Soft Matter*, 2010, **6**, 4788–4799.
119 Q. Zhao, D. W. Lee, B. K. Ahn, S. Seo, Y. Kaufman, J. N. Israelachvili and J. H. Waite, *Nat. Mater.*, 2016, **15**, 407–412.
120 S. H. Woo, Y. J. Mo, Y. I. Lee, J. H. Park, D. Hwang, T. J. Park, H. Y. Kang, S. C. Park and Y. S. Lee, *J. Invest. Dermatol.*, 2023, **143**, 2295–2310.
121 Y. Gouriou, M. R. Alam, Z. Harhous, C. Crola Da Silva, D. B. Baetz, S. Badawi, E. Lefai, J. Rieusset, A. Durand, R. Harisseh, A. Gharib, M. Ovize and G. Bidaux, *Cells*, 2020, **9**, 2542.
122 S. Rana, S. D. Burke and S. A. Karumanchi, *Am. J. Obstet. Gynecol.*, 2022, **226**, S1019–S1034.
123 J. Y. Ji, D. Y. Ren and Y. Z. Weng, *Int. J. Nanomed.*, 2022, **17**, 3163–3176.
124 K. Shankhdhar, *Adv. Skin Wound Care*, 2021, **34**, 1–4.
125 J. Li, Y. P. Zhang and R. S. Kirsner, *Microsc. Res. Tech.*, 2003, **60**, 107–114.
126 M. Marx, R. A. Perlmutter and J. A. Madri, *J. Clin. Invest.*, 1994, **93**, 131–139.
127 K. McLellan, J. S. Petrofsky, G. Bains, G. Zimmerman, M. Prowse and S. Lee, *Med. Eng. Phys.*, 2009, **31**, 165–172.
128 R. S. Kirsner, G. Yosipovitch, S. Hu, A. Andriessen, J. R. Hanft, P. J. Kim, L. Lavery, L. Meneghini and L. C. Ruotsi, *J. Drugs Dermatol.*, 2019, **18**, 1211–1217.
129 M. Jiang, X. Jiang, H. Li, C. Zhang, Z. Zhang, C. Wu, J. Zhang, J. Hu and J. Zhang, *Front. Immunol.*, 2023, **14**, 1136098.
130 S. Guseva, V. Schnapka, W. Adamski, D. Maurin, R. W. H. Ruigrok, N. Salvi and M. Blackledge, *J. Am. Chem. Soc.*, 2023, **145**, 10548–10563.
131 H. Obayashi, R. Wakabayashi, N. Kamiya and M. Goto, *Chem. Commun.*, 2023, **59**, 414–417.
132 A. A. Hyman, C. A. Weber and F. Jülicher, *Annu. Rev. Cell Dev. Biol.*, 2014, **30**, 39–58.
133 S. F. Banani, H. O. Lee, A. A. Hyman and M. K. Rosen, *Nat. Rev. Mol. Cell Biol.*, 2017, **18**, 285–298.
134 J. Berry, C. P. Brangwynne and M. Haataja, *Rep. Prog. Phys.*, 2018, **81**, 046601.
135 Y. Wen and J. Ma, *Front. Immunol.*, 2022, **13**, 986589.

136 E. W. Hester, S. Carney, V. Shah, A. Arnheim, B. Patel, D. Di Carlo and A. L. Bertozzi, *Proc. Natl. Acad. Sci. U. S. A.*, 2023, **120**, e2306467120.
137 E. Cammarota, C. Soriani, R. Taub, F. Morgan, J. Sakai, S. L. Veatch, C. E. Bryant and P. Cicuta, *J. R. Soc., Interface*, 2020, **17**, 20190803.
138 S. Chen, J. Yang, Y. Wei and X. Wei, *Cell Mol. Immunol.*, 2020, **17**, 36–49.
139 A. T. Rowland, D. N. Cacace, N. Pulati, M. L. Gulley and C. D. Keating, *Chem. Mater.*, 2019, **31**(24), 10243–10255.
140 W. E. G. Müller, F. J. Romero, S. Perović, G. Pergande and P. Pialoglou, *J. Brain Res.*, 1996, **37**, 575–577.
141 D. Zwicker, M. Decker, S. Jaensch, A. A. Hyman and F. Jülicher, *Proc. Natl. Acad. Sci. U. S. A.*, 2014, **111**, E2636–E2645.
142 C. F. Lee, C. P. Brangwynne, J. Gharakhani, A. A. Hyman and F. Jülicher, *Phys. Rev. Lett.*, 2013, **111**, 088101.
143 S. K. Vogel, C. Wölfer, D. A. Ramirez-Diaz, R. J. Flassig, K. Sundmacher and P. Schwille, *Cells*, 2020, **9**, 1432.
144 B. Yao, J. Xie, N. Liu, T. Hu, W. Song, S. Huang and X. Fu, *Cell Death Dis.*, 2019, **10**, 272.
145 V. B. Morhenn, T. E. Nelson and D. L. Gruol, *J. Dermatol. Sci.*, 2013, **72**, 87–92.
146 W. E. G. Müller, H. C. Schröder, H. Ushijima, J. Dapper and J. Bormann, *Eur. J. Pharmacol.*, 1992, **226**, 209–214.
147 W. E. G. Müller, E. Tolba, S. F. Wang, M. Neufurth, I. Lieberwirth, M. Ackermann, H. C. Schröder and X. H. Wang, *Sci. Rep.*, 2020, **10**, 17147.

 